

Instituto Tecnológico y de Estudios Superiores de Monterrey

Campus Monterrey

School of Engineering and Sciences



Biogenic silica as a novel carrier to encapsulate isorhamnetin using a
microfluidic device

A thesis presented by

Elena Ivonne Mancera Andrade

Submitted to the

School of Engineering and Sciences

in partial fulfillment of the requirements for the degree of

Master of Science

In Biotechnology

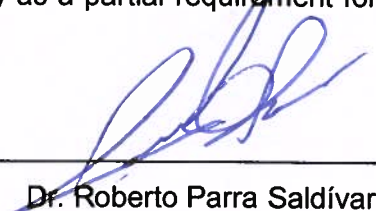
Monterrey Nuevo León, May 14th, 2018

Instituto Tecnológico y de Estudios Superiores de Monterrey

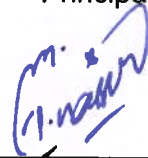
Campus Monterrey

School of Engineering and Sciences

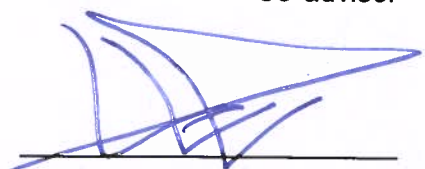
The committee members, hereby, certify that have read the thesis presented by Elena Ivonne Mancera Andrade and that it is fully adequate in scope and quality as a partial requirement for the degree of Master of Science in Biotechnology,



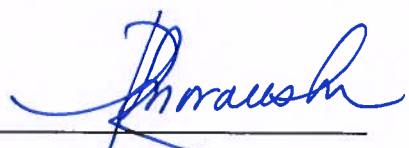
Dr. Roberto Parra Saldívar
Tecnológico de Monterrey
Principal Advisor



Dr. Hafiz M.N. Iqbal
Tecnológico de Monterrey
Co-advisor



Dr. José Guillermo González Valdez
Tecnológico de Monterrey
Committee Member



Dr. Rubén Morales Menéndez
Dean of Graduate Studies
School of Engineering and Science

Monterrey Nuevo León, May 14th, 2018

Declaration of Authorship

I, Elena Ivonne Mancera Andrade, declare that this thesis titled, "Biogenic silica as a novel carrier to encapsulate isorhamnetin using a microfluidic device" and the work presented in it are my own. I confirm that:

- This work was done wholly or mainly while in candidature for a Master of Science degree at this University.
- Where any part of this thesis has previously been submitted for a degree or any other qualification at this University or any other institution, this has been clearly stated.
- Where I have consulted the published work of others, this is always clearly attributed.
- Where I have quoted from the work of others, the source is always given. With the exception of such quotations, this thesis is entirely my own work.
- I have acknowledged all main sources of help.
- Where the thesis is based on work done by myself jointly with others, I have made clear exactly what was done by others and what I have contributed myself.



Elena Ivonne Mancera Andrade
Monterrey Nuevo León, May 14th, 2018

@2018 by Elena Ivonne Mancera Andrade
All rights reserved

Dedication

To my grandparents Elena, José, Josefina, and Gelacio, without you and your wisdom it would not have been possible to have the values and education that you, through my parents, have given me. Thank you for telling me that education will take me further and will give me the opportunities to see the world. I wish you were here, but I know that you are all happy to see this success.

Acknowledgements

I would like to express my deepest gratitude to God because through different people I can see His love and blessings, and with His strength I was able to fulfill my thesis project and courses. I want to thank my mom, dad, and siblings who have been with me in this phase of my life. Thank you for encouraging me every day and support all my decisions. Thank you for all your positive and inspiring words. Thank you for giving me confidence to take tough decisions. It has been hard to have you far away from me, but your love and advices cross frontiers.

To Fede, the love of my life, and my partner in my crazy adventures of life. You have encouraged me to go further in my personal and professional life and helped me have confidence in my knowledge. I'm thankful that you have been with me side by side from the beginning of my career until now. Thank you for all the lessons and advices. To Liz and Fede for all your support.

To my MBI friends Vero, Ramón, Ale, Sara, Maggie, Loren, Alex, Alonso, and Gaby because the courses and the work on the lab were easier and funnier with you. Thank you for all the laughs, jokes, lunches at centrales, and study nights.

To my dear friends Dany, Nahir, Cáder, Anacely, Karenn, Rafa, Paty, Omar, Astrid, Gaby, Fátima, Allamil, JP, Maribel, Paulo, Uli, Karla, Wendy and Marco for being my closest friends in Monterrey. Thank you for being my spiritual pillar and my adventure partners in these eight years.

To "The Fellowship" because you have been there since the beginning of my biotech life. I thank you for being an example and encouraging me to go further in my scientific career.

To Dr. Gregory Rorrer, for giving me the opportunity to have an international experience at OSU. I learned not only how to improve my technical skills, but also to improve my analytical thinking. This opportunity allowed me to have a moment to think clearly about my personal and professional life. It was a challenge, but your support and advices helped me go through it.

To my OSU friends Maggie, Omar, Paul, Joe and Altan. You were of great support during my stay at Corvallis. Thank you for being my friends and to help me get used to the city, to show me the lab, to help me in my experiments and to be patient with me.

To my Corvallis friends Elise, Melanie, Paty, Melissa, Kristina, David Lach, David Leon, Connor, Isaiah, Andrew, John, Brooke, Emma, Hanna, Ellen, Shikha, Valerie, Katie, EJ, Wendy, Jim, Xulei and Antonio. Thank you for being there to help me with my cultural shock, for showing me around, and for being my support in these months.

To Dr. José Rodríguez for being my friend, and helping me with technical questions, giving me support and laughing with me when my experiments went wrong. I really appreciate your honest friendship.

To Dr. Roberto Gallo for helping me with the microfluidic device troubleshooting. Thank you for listening to my ideas and making me solve the technical problems with the device.

To Saúl and Diego for your honest friendship and for giving me all the advices in difficult times.

To Rashmi for being my friend and supporting me with my thesis project. For your valuable support in the conference, advices and for taking care of me.

To Ali for introducing me to a new way to do research, and for helping me with my thesis project.

To CDA staff Luz Elena, Andrea, Abraham and Don Mele for help me with questions on the execution of my experimental work, use of equipment and to have good laboratory practices. Thank you for being with me during my critical work and giving me positive words to finish my experiments. I have learned a lot from you.

To Dr. Hafiz Iqbal for your valuable support in the analysis of results and the execution of my experiments, thank you for being a pillar during my thesis project.

To Dr. Roberto Parra for giving me the opportunity to be his student and the freedom to choose the topic I liked. Thank you for believing in me and giving me confidence on my knowledge. Thank you for your support in all aspects of the execution of my experiments and data analysis.

To Tecnológico de Monterrey support on tuition and CONACyT with the support for living expenses (No. 446209).

Biogenic silica as a novel carrier to encapsulate isorhamnetin using a microfluidic device

By Elena Ivonne Mancera Andrade

Abstract

Diatoms have the peculiarity to synthesize amorphous silica around the cell wall. Frustules (empty silica shells) have the advantages of being biocompatible, biodegradable, nontoxic and rich with OH groups on the surface. Frustules have been used in diverse fields, but recently their application in the biomedical field has been investigated. Drug delivery systems (DDS) have been studied to improve the therapeutic effect of different drugs, especially hydrophobic drugs. Different encapsulation methodologies have been used to load the drug in a carrier such as drop-wise methodology or solvent evaporation. However, a reproducible methodology that reduces handling error must be explored. In the present work, a microfluidic device is used as a novel encapsulation technique for solid particles and hydrophobic drugs. A novel microfluidic device fabrication technique was used: ESCARGOT (Embedded SCAffold RemovinG Open Technology). Isorhamnetin was used as a model drug which has a hydrophobic nature. Three different concentrations were studied: 20, 60 and 100 µg/mL, and three different resident times in the device (0.4, 1 and 2 minutes). The highest encapsulation efficiency (EE%) and loading capacity (LC%) were 17.92% and 1.63% respectively. According to the statistical analysis, the optimum conditions to obtain a maximum (EE%) were 2 minutes and 20 µg/mL. The isorhamnetin release behavior was observed with a burst release in the first hour with 48.26%, while the total amount of drug was delivered in three hours. The feasibility of frustules as carriers and the microfluidic device as a mixer was successfully accessed. This methodology could be used as a standardization technique to obtain reproducible results. Further studies with frustule surface functionalization need to be performed to improve EE%.

Keywords: Microfluidic device, frustule, isorhamnetin, drug delivery

Table of contents

Abstract.....	vi
List of Figures	ix
List of Tables	x
Chapter I.....	1
1. Introduction	1
1.1 Hypotheses.....	3
1.2 General objective	3
Chapter II.....	4
2. Theoretical framework	4
2.1 Diatom generalities.....	4
2.2 Applications in drug delivery.....	9
2.3 Microfluidic device.....	12
2.4 Isorhamnetin	13
Chapter III.....	14
3. Materials and methods.....	14
3.1 Chemicals and reagents	14
3.2 Diatom cultivation.....	14
3.3 Frustule isolation and preparation	16
3.4 Frustule characterization	18
3.5 Manufacturing of the microfluidic device.....	19
3.6 Isorhamnetin encapsulation	20
3.7 Isorhamnetin release kinetics	21
Chapter IV	23
4. Results and discussion	23
4.1 Diatom cultivation.....	23
4.2 Frustule cleaning.....	24
4.3 Frustule characterization	26
4.4 Isorhamnetin encapsulation	29
4.5 <i>In vitro</i> isorhamnetin release	35
Chapter V	37
5. Conclusions	37
References	39
Annex A.....	46

Design of experiments	46
Statistical analysis for encapsulation efficiency.....	47
ANOVA for selected factorial model	47
Optimization	48
Statistical analysis for loading capacity.....	48
ANOVA for selected factorial model.....	48
Optimization	49
Annex B	50
Abbreviation list.....	50
Published papers.....	51
Book Chapter	52
VITA.....	53

List of Figures

Figure 1. Schematic representation of diatom cell	2
Figure 2. Frustule applications	5
Figure 3. Schematic representation of centric diatoms	7
Figure 4. Schematic representation of cell reproduction	7
Figure 5. Schematic representation of diatom shapes	8
Figure 6. Schematic representation of microfluidic channels	12
Figure 7. Isorhamnetin structure	13
Figure 8. The schematic assembly of the photobioreactor	16
Figure 9. Microfluidic device design	19
Figure 10. Microfluidic device	20
Figure 11. <i>Cyclotella</i> sp. growth kinetics	24
Figure 12. Frustule isolation methodologies	26
Figure 13. <i>Cyclotella</i> sp. SEM images	27
Figure 14. Frustule element analysis	28
Figure 15. The typical FT-IR spectra of frustules	29
Figure 16. Encapsulation efficiency (%)	31
Figure 17. Loading capacity (LC%)	32
Figure 18. FT-IR spectra of isorhamnetin encapsulated	34
Figure 19. Isorhamnetin encapsulation in different concentrations	35
Figure 20. Drug release (%)	36

List of Tables

Table 1. Physicochemical characteristics of frustules	4
Table 2. Organisms used for drug delivery applications	11
Table 3. Retention time and drug concentration used	20
Table 4. Organic material removal	26
Table 5. Comparative drug encapsulation	33
Table A1. Design of experiments	46
Table A2. ANOVA for factorial model: encapsulation efficiency	47
Table A3. Fit Statistics	47
Table A4. Optimization for encapsulation efficiency	48
Table A5. ANOVA for factorial model: Loading capacity	48
Table A6. Fit Statistics	49
Table A7. Optimization for loading capacity	49
Table B1. Abbreviation list	50

Chapter I

1. Introduction

The biological formation of inorganic materials with complex form, e.g., biosilica is a widespread phenomenon in nature. Biosilica is an alternative source for the production of silica particles that may be used as carriers with noteworthy potentialities for several applications including drug delivery. In comparison with synthetic silica, biosilica is naturally ordered with a multilayer and well-defined nanoporous structure. One of the main drawbacks of synthetic silica particles is the difficulty in obtaining particles with highly ordered porosity, uniform pore size, and possible toxic by-products obtained due to the manufacturing process [1]. Thus, biosilica obtained from diatom microalgae and marine sponges provide no toxicity, exhibits biocompatibility and biodegradability. Diatoms are being the world's largest contributors of biosilification in water bodies with a production of 240 T mol Si/year which represents 45% of the total oceanic primary production of silica [2], [3]. There is an estimation of living algae from 30,000 to more than 1 million species; only 72,500 have been identified from which 20,000 corresponds to diatoms [4]. There are different complex morphologies of diatoms which have been classified as centric and pennates. Centric diatoms have radial symmetry, while pennates have an elongated shape. The transparent amorphous silica is formed around the cell wall during the reproduction cycle, and it can have varied sizes that are directly correlated with the species. Silaffins, silacidins, and long-chain polyamines (LCPA) present in the silica deposition vesicle (SDV) are the responsible molecules for the silica synthesis (Figure 1). Biosilica is obtained when the organic material is removed through well-established protocols such as acid, surfactant, and thermal treatments [5]–[8]. The above-mentioned novel features offer candidature of diatoms in different areas, but specifically, as remarkable carriers for biomedical applications.

The high-tech advancements in polymer science offer notable potentialities which led to their exploration as a novel carrier in drug delivery systems (DDS). Drug delivery can be defined as a sustained distribution of drugs in a controlled way at a specific target site [9]. The controlled delivery is achieved by taking advantage of the biochemical characteristics of a drug-loaded carrier and environment of the target site. This also additionally benefits an effective drug exposure which maintains the drug in the tissue for longer times giving, in this way, a broad therapeutic window. The attachment or encapsulation of the drug in a carrier allows the protection of it in the physiological environment. The main advantages of encapsulation are the enhancement of sensitivity of tumor tissue to drugs, the increment of the drug solubility,

bioavailability, drug stability, prolonged half-life, reduction of dose, and the possibility to include two or more drugs into the same carrier [10]–[12]. This allows having an effective therapy and a reduction of side effects due to the selectivity of the delivery. Diverse types of carriers have been studied such as liposomes [13], biodegradable materials such as PLGA [14], polymeric micelles [15], metallic materials [16], dendrimers [17], nanotubes [18], and silica particles [19]. Among these, silica (silicon dioxide, SiO_2) exhibits proper characteristics for its use in the biomedical area such as biocompatibility, biodegradability, capacity to change surface chemistry, chemical stability, and large surface area for sorption processes [20]–[22].

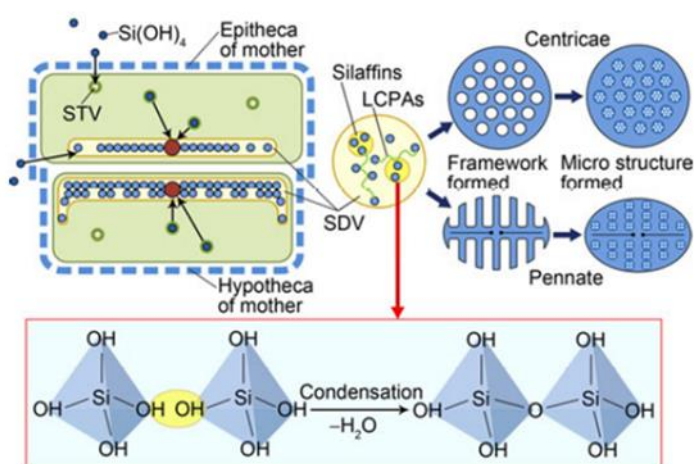


Figure 1. Schematic representation of diatom cells. Reproduced from Zhang et al., 2012 [23], an open access paper published under Creative Commons license.

Several methodologies have been reported to encapsulate biomolecules or drugs, though the use of different carries that involve adsorption or covalent binding reactions. The most common methodologies involve stirring and/or evaporation steps to permit the interaction with the drug and the carrier electrostatic forces. The main advantages of traditional methodologies are the one-step adsorption process, easiness, and higher contact between the drug and the carrier. However, adsorption processes are time consuming (several hours), depending on the carrier material, hydrophilic drugs are difficult to incorporate; and some of them use toxic solvents [24].

A novel approach using a microfluidic device can be addressed to improve drug loading, production of tailor-made particles, and encapsulation of one or more drugs with different natures (hydrophobic or hydrophilic) [25]. Microfluidics study the manipulation of fluids in channels with the size of micrometers to study their behavior [26]. Different configurations can be designed to

study the behavior of the fluids. One of the main advantages is the creation of microsystems by changing parameters such as flow rate and channel dimensions, among others. A microfluidic device could be used as a mixer, particle manufacturer or as a bioreactor. Lithography is the main technique used for the manufacture of microfluidic devices, although it is expensive and requires the use of specialized equipment and specific training. Researchers have developed a novel, easy and less expensive technique for the manufacture of a microfluidic device called ESCARGOT: Embedded SCAffold RemovinG Open Technology [27]. It involves the microfluidic design printed in 3D as a mold and its curation using PDMS polymer. Hence, in the present work, the use of biogenic silica from frustules to encapsulate a model drug through a microfluidic device (manufactured with the ESCAGOR methodology) was evaluated.

1.1 Hypotheses

- Biogenic silica obtained from diatom microalgae are efficient carriers for isorhamnetin encapsulation.
- A microfluidic device is capable to perform isorhamnetin encapsulation into biogenic silica.
- Isorhamnetin encapsulated into biogenic silica shows a controlled release.

1.2 General objective

This work aims to evaluate the technical feasibility of *Cyclotella sp.* frustules as a carrier for the encapsulation of isorhamnetin using a newly designed microfluidic device.

1.2.1. Specific objectives

- To cultivate *Cyclotella sp.* in a bubble 5L photobioreactor under controlled environment.
- To evaluate the influence and efficacy of different cleaning methodologies, i.e., acidic, surfactant or thermal methodology.
- To characterize different parameters including morphology, elemental analysis, and size by scanning electron microscopy and Fourier transform infrared spectroscopy.
- To design and develop a microfluidic device using the ESCARGOT methodology.
- To encapsulate isorhamnetin in frustules under different conditions.
- To evaluate *in vitro* isorhamnetin delivery in a simulated fluid.

Chapter II

2. Theoretical framework

2.1 Diatom generalities

The term algae refers to all photosynthetic organisms, different from plants, which comprise diverse sizes ranging from micrometers to meters called microalgae and macroalgae respectively. There is an estimation of living algae on the planet that varies from 30,000 to more than 1 million species. From all types of algae, there is a specific group that has the peculiarity of synthesizing silica around the cell wall called diatoms, from which around 20,000 species have been described [4]. Diatoms have been found in marine and freshwater ecosystems as well as in soil. Round et al., classified diatoms according to their morphology in three classes: *Bacillariophyceae*, *Coccolodiscophyceae*, and *Fragilariophyceae* [28]. However, other species belong to *Chrysophyceae*, *Dictyochophyceae*, *Mediophyceae*, among other classes.

Once diatoms are harvested from the culture, an organic matter removal protocol is applied. Several studies have been performed by using hydrogen peroxide and hydrochloride acid, surfactants, and thermal treatments. The clean silica exhibits wide physicochemical characteristics that make them suitable for diverse applications such as biofuel production, synthetic biology, biocatalysis, among others (Table 1, Figure 2). Their special property of silica synthesis with interesting properties has opened a new field of research in biomaterials and molecular science.

Table 1. Physicochemical characteristics of frustules.

Physicochemical characterization
Biocompatible
Biodegradable
Non-toxic
Chemically inert
Ease surface functionalization
Nanoporosity
Mesoporous material
Large surface area
High concentration of lipids
Complex morphology
Optical properties

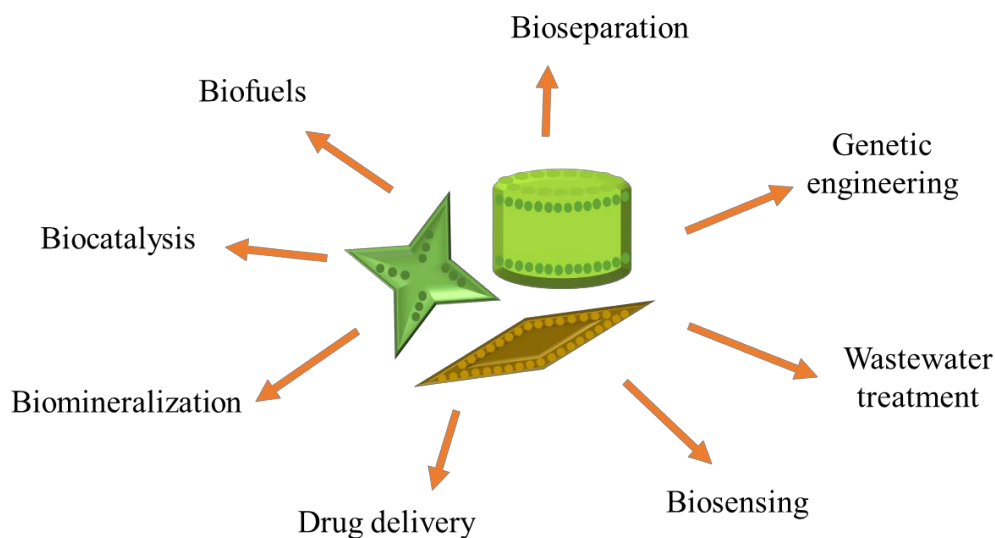


Figure 2. Frustule applications.

2.1.1 Sources

As mentioned, diatoms are living eukaryotic organisms that may be found in freshwater, oceans, and soil. Two types of diatom organisms have been used for different applications: diatomaceous earth (DE) and living organisms. Living organisms use the silicic acid (silica precursor) available in the environment to synthesize the frustule and valves during cell division. Once diatoms reach the death phase, the frustule either dissolves and serves as a source for other diatoms, or precipitates and remains in the sediment of the water body. DE are fossilized diatoms found in the sediment of water bodies. The main difficulties of working with DE is the irregular shapes and sizes due to a mixture of distinct species. In this regard, a previous homogenization process such as pulverization or sonication needs to be performed to obtain smaller sizes, and a filtration process needs to be applied to acquire size uniformity. Interesting attempts to apply emerging technologies such as electric pulses have been used to obtain a purer and porous structure of DE [29]. Hence, working with living organisms has the advantage of selecting the desired morphology (centric or pennate) and size according to the final application.

2.1.2 Phylogeny

Diatoms come from different ancestors. It has been identified that centric diatoms appeared in the early Cretaceous, while pennates diatoms were recorded in the late Cretaceous.

Studies suggested that motile pennates (raphid) evolved first in the middle of the Eocene, while non-motile pennates (araphid) evolved later [30]–[33]. One of the most accepted hypothesis is that the first diatom cell, a naked photosynthetic cell, lacked the silica shell, and through time the silica shell was acquired. After that, the diatom cell with a silica shell developed the valves and girdle bands [28]. Phylogenic trees have been proposed with different hypothesis about the relationship of species. However, one of the main difficulties are the different approaches of traditional and standard studies used to analyze and unify the information recovered. While the standard phylogenetic study compares all the characters across all taxa, the traditional approach focuses on one characteristic in one taxon at a time [34]. In this regard, the complexity of phylogenic studies has made it difficult to either classify or establish a unique phylogenetic tree for diatoms.

2.1.3 Reproduction

Diatoms have a unique reproduction cycle that differs from the rest of microalgae which use binary fission to divide. In the first stage, diatoms use binary fission and separate the upper and bottom valves of the cell called epitheca and hypotheca respectively (Figure 3). Once they are separated, peptides involved in the biosilification process start synthesizing either the epitheca or hypotheca of the daughter cell (Figure 4). Cells divide and synthesize silica valves until they reach a critical size which is normally below half of the regular size. At this point, diatoms cells restore their size and the binary fission is switched to the start of the sexual reproduction. After meiosis of female and male cells, fertilization takes place to form a zygote. The zygote will increase its size by the uptake of water from the environment forming an auxospore; at the end of this process, the cell has almost its original size. The auxospore is divided several times until the normal size is reached. During this division, the cell discards both halves to free the protoplast which will grow again until a normal cell size is reached. After that, the auxospore synthesizes the halves again. In this way, diatom cells restore their size and start the cellular cycle again. This cell cycle was hypothesized by MacDonald & Pfister, but it was Geitler who refined the understanding of size variation at which sexual reproduction begins, and that this is strongly dependent of the taxon [35]–[37]. A variance in the sexual reproduction of centric and pennates diatoms has been established. Centric undergo by morphological oogamy where a large non-motile egg is fertilized by a flagellated motile sperm; while pennates occur by two types: morphological isogamy (raphid pennates, motile) and physiological anisogamy (araphid pennates, non-motile). In pennate cells, the gametes are non-flagellated and are brought together by a prior pairing of their mother cells [38].

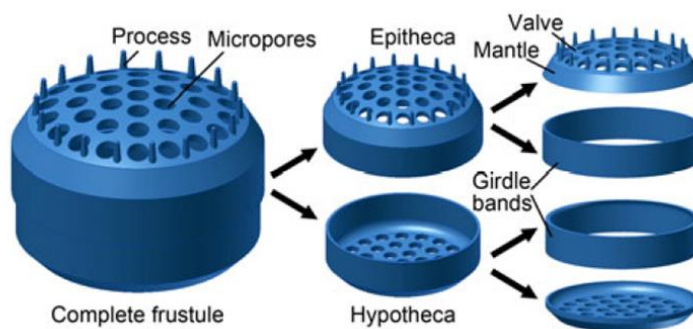


Figure 3. Schematic representation of centric diatoms. Reproduced from Zhang et al., 2012 [23], an open access paper published under Creative Commons license.

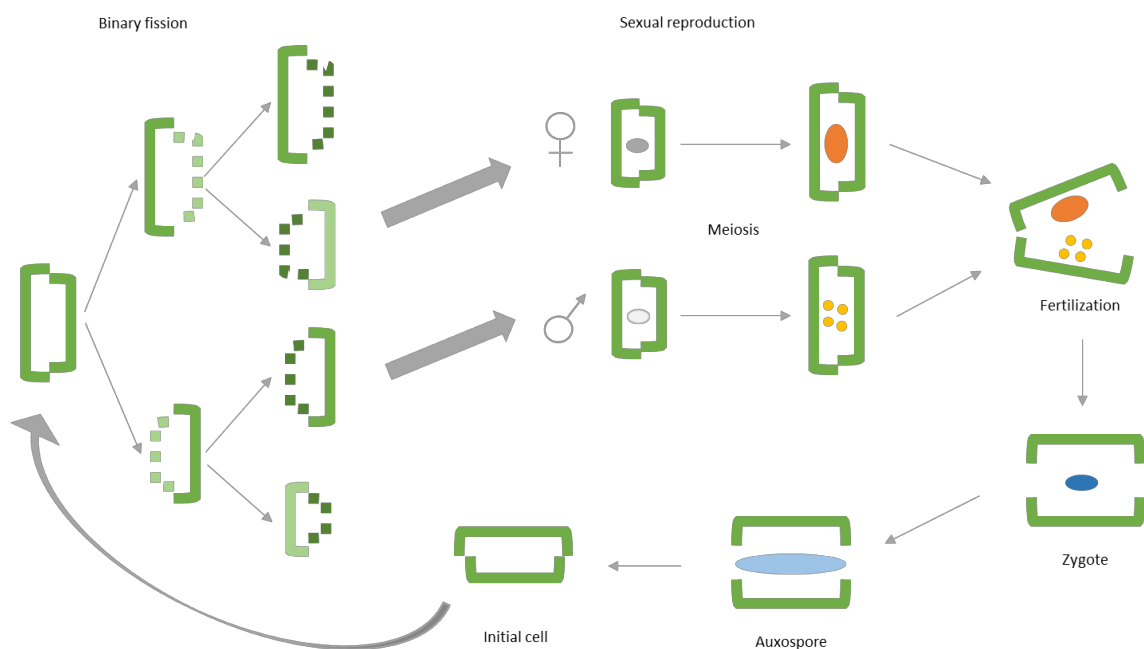


Figure 4. Schematic representation of cell reproduction.

As previously mentioned, diatoms use the silicic acid available in water as a silica precursor. Silicic acid transporters, transmembrane proteins, are in charge of transporting the silicic acid inside the cell where it is deposited in the silica deposition vesicle (SDV). The SDV is located near the cytoplasmic membrane of the cell. Silaffins, long-chain polyamines (LCPA) and silacidins, specific peptides, are in charge of synthesizing the silica through polymerization and

hydrolysis reactions between the silicic ions at an acid environment ($\text{pH} \approx 4.5$) (Figure 1). The first step taken is when the SDV is widened while the framework structure of the frustule is formed which usually takes several minutes. Then, the structure becomes thicker as well as the SDV, and the valves are developed (several hours) [23]. It is known that the pattern and shape are directly affected by these peptides during the synthesis. Hence, diatoms differ from the quantity and type of peptides that are found in the SDV. Some species only possess silaffins while others possess up to 20 different forms [39]. It has been studied that one of these peptides can synthesize silica alone through a condensation reaction, however, the presence of LCPA reduces the synthesis time and can influence the final morphology of the cell [40].

Even when studies have been performed to understand the mechanisms under which silica is synthesized, a lack of information regarding the internal silica pool mechanisms is still present.

2.1.4 Morphological characterization

Diatom morphology and size depends strictly on the species and it can vary from 2 to 2000 μm . Diatoms have been classified in two main classes: centric and pennates; but a third classification has been proposed for those species with a complex morphology. As previously mentioned, centric diatoms have a symmetrical and radial shape, while pennates have a zygomorphic structure. Complex morphologies are three-dimensional structures with irregular shapes (Figure 5). Centric and pennate frustules are composed of two joined valves (epitheca and hypotheca) by girdle bands.

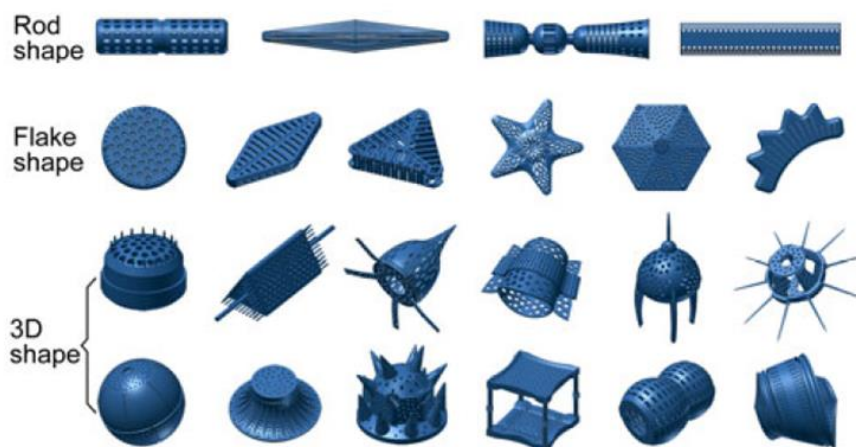


Figure 5. Schematic representation of diatom shapes. Reproduced from Zhang et al., 2012 [23], an open access paper published under Creative Commons license.

2.2 Applications in drug delivery

Biogenic silica has been known for decades, however, it has attracted large attention in the past years. Its complex morphology and physicochemical characteristics makes these materials candidates for different applications. Biofuels, synthetic biology, heavy metal entrapment, agriculture and other applications have been widely studied. Though, biogenic silica in drug delivery applications has recently emerged. Drug delivery has attracted the attention of researchers due to the promising goal of producing non-invasive therapies to treat different diseases. For instance, in cancer therapies, the aim of drug delivery is to transport a mixture of drugs embedded in a carrier to a specific location in the body. Once the carrier has reached the desired location, the drugs are liberated through a diffusive process due to biodegradation of the carrier [9].

Drug encapsulation into micro or nanocarriers has proved the enhancement of drug solubility, specially of poor soluble drugs; and provides protection for the drug in the physiological environment [12]. One of the principal concern points in the production and synthesis of carriers is the use of toxic solvents and complex methodologies, and uniform particle size production, followed by the expensive production cost, considerable amounts of energy and time required. Hence, the use of biogenic silica seems to solve these obstacles. As mentioned in Chapter I, biogenic silica comprises advantageous properties such as compatibility, biodegradability, high surface area, thermal, stability, chemical inertness, controlled drug release, low density and easy surface modifications [3]. The highly ordered nanopores and the available OH groups in the surface make it a suitable material to encapsulate drugs. A study with drugs that treat gastrointestinal diseases evaluated the encapsulation of these molecules and was performed in DE. The LC% of mesalamine and prednisone achieved were 11.5% and 9.9% respectively. However, the drug release studies showed an abrupt release of the 80% of the encapsulated mesalamine in one hour, while 67% was reached with prednisone in a simulated gastric fluid. After two hours, mesalamine was completely released while prednisone reached a 33%. Also, a slower release was observed with prednisone in comparison with mesalamine. An *in vitro* study with Caco-2/HT-29 cell lines was performed, and the results showed an increment of drug permeation through the monolayer of the cell. Since the drug concentration in the gastric system needs to be controlled due to side effects at high concentrations, the controlled permeation achieved with the delivery of the drug thought time could reduce the side effects on patients [41]. In cancer therapy, the encapsulation of a small interfering ribonucleic acid (siRNA) in human lung epidermoid cancer cells (H1355) was evaluated [42]. In this case, the researchers wanted to use nanoparticles (NPs) and DE was crushed to obtain a size lower than 450 nm. Interestingly, NPs

were functionalized with amine groups to attach the drug covalently and improve the EE%. The cytotoxic effect on cancer cells (HeLa cell line) of magnetic frustules *from Nitzschia sp.* with encapsulated curcumin was evaluated. Curcumin release was fast in the first 12 h, while it maintained a slow release up to 24 h where most of the drug was released (98.6%). The highest cytotoxicity rate calculated was 60.2% with magnetic particles, while a non-magnetic particle reached 44.8%. Researchers discussed a synergetic effect between the magnetic material and the curcumin to achieve the highest cytotoxic effect, while the frustules did not showed any cytotoxic effect [3]. *In vivo* studies performed on mice with an aluminum surface modification of DE particles showed no toxicological reaction during the period of evaluation of the anti-inflammatory drug [43]. Studies with *Coscinodiscus concinnus* frustules were used to deliver streptomycin *in vitro*. Frustules and functionalized frustules had 78% and 65% of drug release in 6 h respectively and maintained a sustained release up to 3 and 7 days respectively. The addition of hydroxyl groups in the surface allowed the increment of drug adsorption [44].

As seen in Table 2, fewer studies with frustules from living algae have been reported, hence there is an opportunity for further studies. Additional studies regarding surface functionalization of frustules and the encapsulation of two or more drugs in the same silica particle, particle stabilization as well as *in vivo* studies must be performed.

Table 2. Organisms used for drug delivery applications. It is shown applications of frustules in drug delivery. D : diameter, L: length, LC: loading capacity, EE: encapsulation efficiency.

Organism	Average size	Drug	DL and EE	Therapeutic use	Ref.
Diatomaceous earth	D= 4-6 μ m L= 10-20 μ m	Indomethacin	LC = 21% EE = 94%	Anti-inflammatory	[45]
Diatomaceous earth	D = 4-6 μ m L = 10-20 μ m	Indomethacin and gentamicin sulfate	LC = 14-22%	Anti-inflammatory and antibiotic	[46]
Diatomaceous earth	L = 33.5 μ m	Diclofenac sodium	LC = 90%	Anti-inflammatory	[43]
Diatomaceous earth	1 - 50 μ m	Carbamazepine	-	Psychomotor seizures and trigeminal neuralgia treatment	[47]
Diatomaceous earth	D = < 450 nm	siRNA		Gene silencing in cancer cells	[42]
Diatomaceous earth	D= 10 μ m L = 10-20 μ m	Mesalamine and prednisone	LC mesalamine = 11.5% LC prednisone = 9.9%	Gastrointestinal therapy	[41]
<i>Nitzschia</i> sp	L = 1.3 - 8 μ m	Curcumin	EE = from 41 – 73% LC = 9.1% - 14.7%	Chemotherapy	[3]
<i>Coscinodiscus concinnus</i>	-	Streptomycin	LC = 33%	Antibiotic	[44]

2.3 Microfluidic device

Microfluidics is a science that studies the manipulation of fluids in microchannels. Due to the small chemical amounts needed and the easiness to change experimental parameters (flow rate, solvents, etc.), different microsystems can be created [26]. Microfluidic devices can be used as mixers, bioreactors and particle manufacturers. Recently, the droplet-based microfluidic technique has been explored to manufacture micro and nanoparticles and at the same time to encapsulate drugs. Different channel configurations can be used to achieve a desired size, composition and volume by the mixing of two partially miscible or immiscible fluids, or to form multiple emulsions (Figure 6).

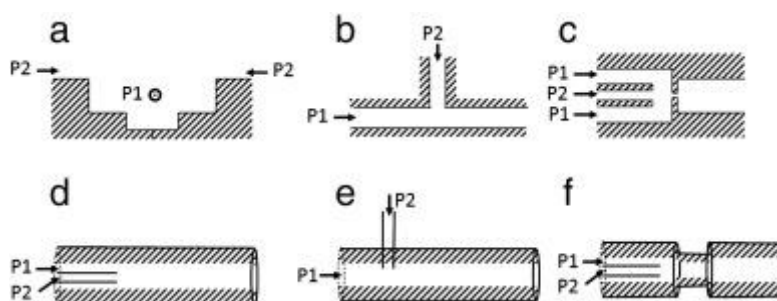


Figure 6. Schematic representation of microfluidic channels. a) terrace-like device, b) T-junction device, b) flow focusing device. c) Capillary-based devices: d) co-flow device, e) cross-flow device, f) flow focusing device. Reproduced from *Journal of Controlled Release*, vol 172(3), I.U. Khan, C.A. Serra, N. Anton and T. Vandamme, *Microfluidics: A focus on improved cancer targeted drug delivery systems*, 1065-1074, Copyright (2013), with permission from Elsevier. [48]

The main advantages to use a microfluidic device are the improvement on mass and heat transfer between the fluids, millisecond mixing times, high surface to volume ratios, laminar flows, small amounts of reagents needed and the easiness to create rapid libraries of materials by changing fluids or modifying concentrations [26],[48]. Different methodologies are used for the fabrication of a microfluidic device such as micromilling, micromachining, lithography and mold replication [48]. However most of these techniques result expensive, time consuming and use specific technical skills and equipment.

Different materials are used such as silicon, polydimethylsiloxane (PDMS), poly(methyl methacrylate) (PMMA), polycarbonate (PC), cyclic olefin copolymer (COC), polyetheretherketone (PEEK), polyimide plastic resin (PIPR), glass, quartzose and silicon have been used [25]. However, the material selection is dependent of the final application. For instance, for biomedical

applications PDMS is the most used material due to its gas permeability factor, optical transparency in the visible and ultraviolet regions, and surface functionalization [49].

2.4 Isorhamnetin

Flavonoids are phenolic compounds that are commonly found in diverse plants, vegetables and fruits. Usually, these are found as glycosylated or esterified forms with a basic structure consisting of C₆-C₃-C₆ rings with different substitution patterns [50]. The different substitutions can lead to their classification and specify their bioactivity. Isorhamnetin (C₁₆H₁₂O₇, CAS 480-19-3) is a flavonol aglycone that can be extracted from different plants (Figure 7). Endogenous Mexican plants such as *Tagetes lucida* flowers and *Opuntia ficus-indica* contain this flavonol among others. It has been studied that isorhamnetin exhibits different biological activities such as antitumoral [51], anticoagulant [52], anti-inflammatory [53], and anti-thrombotic [54] activities. For instance, *in vivo* studies have shown that the injection of isorhamnetin (0.5 mg/kg) in mice to evaluate the effect in lung tumor. After 13 days, the decrement of tumor size was at least one order of magnitude lower than results obtained with quercetin (flavonol) [55].

In the present work, isorhamnetin was used as a drug model due to its hydrophobic nature and its future evaluation in an integrated bioprocess.

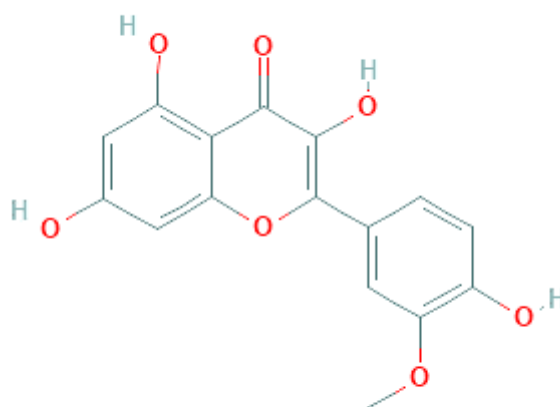


Figure 7. Isorhamnetin structure.

Chapter III

3. Materials and methods

3.1 Chemicals and reagents

Isorhamnetin was purchased from Sigma-Aldrich, USA. SYLGARD silicone elastomer 184 and SYLGARD silicone elastomer 184 curing agent (Dow Corning Corporation, United States) was generously gifted by Dr. Sergio O. Martinez-Chapa from Tecnológico de Monterrey. All other chemicals and reagents were of analytical grade and were purchased from Sigma-Aldrich, USA.

3.2 Diatom cultivation

Cultivation studies were performed at Dr. Gregory Rorrer's laboratory at Oregon State University. *Cyclotella* sp. was obtained from UTEX Culture Collection Algae (UTEX #1269) and cultivated in a 500 mL non-agitated Erlenmeyer flask with 90 mL of Harrison's Artificial Seawater medium enriched with *f/2* nutrients [6], [56] and 10 mL inoculum.

The inoculum medium was comprised of: 347 mM NaCl, 23.8 mM Na₂SO₄, 7.68 mM KCl, 1.97 mM NaHCO₃, 690 μM KBr, 354 μM H₃BO₃, 63.3 μM NaF, 45.1 mM MgCl₂·6H₂O, 8.74 mM CaCl₂·2H₂O, and 78.0 μM SrCl₂·6H₂O. The *f/2* enrichment medium components consisted of 35.9 nM Na₂MoO₄·2H₂O, 0.954 nM Na₂SeO₃, 6.0 nM NiCl₂·6H₂O, 165 nM ZnSO₄·7H₂O, 45.3 nM CuSO₄·5H₂O, 24.7 nM CoSO₄·7H₂O, 2.31 μM MnSO₄·4H₂O, 19.7 μM FeCl₃·6H₂O, and 21.9 μM ethylenedinitrol tetraacetic acid disodium salt (C₁₀H₁₄O₈N₂Na₂·2H₂O). Vitamin solution consisted of 1.15 μM thiamine, 0.0005 nM biotin and 0.004 nM vitamin B12. The macronutrient medium consisted of 5.32 mM NaNO₃, 242 μM NaH₂PO₄·H₂O and 200 mM Na₂SiO₃·9H₂O. Culture media was sterilized by filtration using 0.2 μm pore size filter (VWR Vaccum Filtration Systems, VWR, United States). Cultures were maintained at 22°C, with a light intensity of 50 μE/m²s, and a photoperiod of 14h light and 10 h darkness. The cell suspension was subcultured every 3 weeks with 10% v/v inoculum. After three weeks, the flasks were gathered together in one sterile Erlenmeyer flask under similar conditions. Cell density and cell diameter were measured by triplicate using a cell counter (Z2 Coulter Particle Count and Size Analyzer, Beckman Coulter, United States) with a range of minimum threshold of 6 μm to 19 μm. A dilution factor of 100 was used to measure cell density (100 μL cell suspension and 9.9 mL diluent).

A 5 L bubble column photobioreactor (Figure 8) was used to study the growth kinetics, characteristics and configuration mentioned elsewhere [57]. The culture media for the photobioreactor was the same as mentioned above, but changing the macronutrient solutions to 7 mM NaNO₃, 15 μM NaH₂PO₄·H₂O and 1 mM Na₂SiO₃·9H₂O. These parameters were modified to maintain the pH at 8 because the injection of CO₂ tends to modify the pH towards an acid environment. The bubble column photobioreactor was initially inoculated with 60 mL cell suspension with a cell density of $1.06 \times 10^5 \pm 8.30 \times 10^3$ cells/mL. Filtered air and CO₂ were provided to the photobioreactor at a flow of 2.4 L/min, and 380 ppm respectively. Daily samples were taken to monitor cell density, pH and silicon concentrations in the reactor. During the exponential phase, two samples were taken per day. Samples were taken by using a 60 mL sterile syringe and the volume withdrawn was of 5 mL. Sterile air was injected with the same syringe through the sampling output to remove cells from the sampling tube of the reactor.

When the stationary phase was reached, the cell suspension was kept in starving conditions of two photoperiod cycles to synchronize all cells and to obtain a uniform material [58]. A centrifugation process was performed to harvest the diatoms by using 250 mL vessels and were centrifuged for 10 minutes at 1500 g (IEC CL30, Thermo Electron Corporation, United States).

Dissolved silicon was measured by spectrophotometric assay: 5 mL of sample was mixed with 200 μL of 13% w/v ammonium molybdate solution in water, and 100 μL of 18.7% v/v hydrochloric acid (HCl). The reaction was left still for 10 minutes, 3 mL of sample was transferred to a quartz cuvette and measured at 360 nm [59]. Measurements were performed in duplicate. A dilution factor of 5 with distilled water was used when necessary (1 mL of cell culture supernatant and 4 mL distilled water). A standard curve of six points was done using Na₂SiO₃ as a standard.

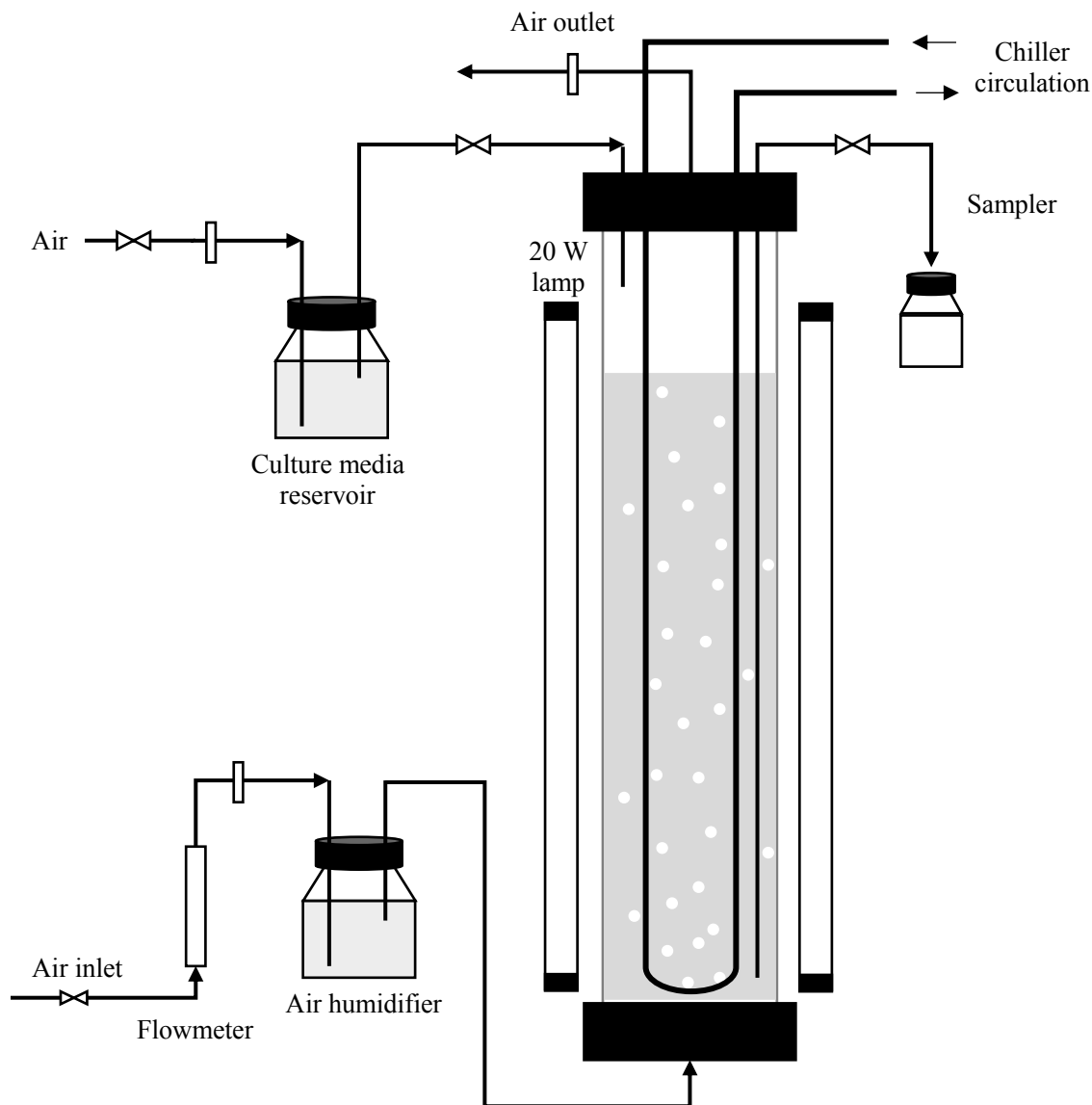


Figure 8. Schematic assembly of the photobioreactor.

3.3 Frustule isolation and preparation

Three isolation processes were performed to determine an optimal and successful organic material removal without compromising the integrity of the frustules. 115 mL of culture media with approximately 1×10^6 cells/mL was centrifuged at 1500 *g* for 15 minutes. Three washes with distilled water were performed, and at the end of the third wash, the pH of the supernatant was measured to verify the acidity of the water indicating the removal of salts. 5 mL of sample were added to pre-dried and weighed Aluminum crinkle dishes to obtain their dry weight at 80°C. Each of the following methodologies was performed.

3.3.1 Hydrogen peroxide and hydrochloric acid methodology

Cells were placed in a 50 mL centrifuge tube following the addition of 29.750 mL of 30% hydrogen peroxide (H_2O_2) and 250 μL of a 37% hydrochloric acid (HCl) solution. The mixture was inverted gently twice to allow the reagents mix with the cells. The centrifuge tube was placed in a vacuum for 1 h to eliminate bubbles. To avoid frustule breakage, the solution was maintained uncapped and without stirring for 42 h at room temperature (22°C). The HCl/ H_2O_2 solution was removed from the centrifuge tube using a pipette, 30 mL of distilled water were added, the mixture was inverted gently to wash cells, and it was left still for 6 h or until cells precipitated. Water washes were performed three times. Subsequently, frustules were washed 3 times with methanol to remove water [6]. Frustules were re-suspended in 10 mL of methanol (96%) and were transferred to a previously weighted glass vial. The vial with frustules was placed in an oven at 80°C for 24 h to determine its dry weight. For SEM visualization, frustules were washed three times with deionized water and were stored in MiliQ water at 4°C until use.

3.3.2 Sodium dodecyl sulfate/Ethylenediaminetetraacetic acid (SDS/EDTA) methodology

Cells previously washed with water were transferred in a 50 mL centrifuge tube. 40 mL of SDS/EDTA (50 g/L SDS in 100 mM EDTA) were added to the tube with the solution, the tube was then vortexed for 1 min, left still for 20 min, and centrifuged at 4,500 rpm for 20 min. This step was repeated three times. After that, frustules were washed 3 times with distilled water, and 3 times with methanol; in both cases, frustules were not left still [8]. Frustules were transferred to a glass vial (weighted previously) and resuspended in 10 mL. The glass vial was placed in an oven for 24 hours at 80°C. For SEM visualization, frustules were washed three times with deionized water and were maintained in MiliQ water and stored at 4°C until use.

3.3.3 Thermal treatment

Washed cells were resuspended in 15 mL of water and were poured in a porcelain capsule (previously weighted). The capsule was placed in a muffle furnace (Thermolyne, Thermo Scientific, United States) for 6 hours at 600°C [5]. After that, porcelain capsule was placed in a desiccator for 30 minutes and weighted. 15 mL of methanol (96%) was added to the porcelain capsule to recover the frustules. Frustules were transferred to a glass vial and were stored at 4°C until use. For SEM visualization, frustules were washed three times with distilled water and were maintained in MiliQ water at 4°C until use.

Intact frustules were visualized using Scanning Electron Microscope (SEM) at 20 kV (EVO MA25, Zeiss, United States), and by comparing dry weight loss between each methodology according to equation 1 and equation 2. The total organic material (TOM) present in the sample was calculated as the initial biomass dry weight minus the ash weight. The ash weight corresponded to inorganic material present in the sample mainly composed of silica and metal traces.

For SEM analysis, pins were covered with carbon tape to attach the sample in the surface. One droplet of each sample was placed in the carbon tape and was let dried in a desiccator. Measurements were taken with a variable pressure mode.

$$TOM = (DWb - DWt) + (DWt - Ash) \quad \text{Eq. 0}$$

$$TOM = DWb - Ash \quad \text{Eq. 1}$$

$$\text{Organic material removal (\%)} = \left(\frac{DWt - Ash}{TOM} \right) * 100 \quad \text{Eq. 2}$$

Where:

TOM: total organic material

DWb: dry weight of biomass before treatment

Ash: weight of the sample after muffle furnace

DWt: dry weight after the treatment

3.4 Frustule characterization

Frustule characterization was performed using SEM (EVO MA25, Zeiss, United States). The sample was placed in the pin using carbon tape to adhere to the surface. One droplet of each sample was placed in the carbon tape and was let dried in a desiccator. 20 kV of voltage and variable pressure were used. With this technique, diatom size, nanopore size, and 3D morphology were determined. The elemental analysis was determined with energy dispersive spectroscopy using a Bruker XFlash 6/10 detector with a 20 kV accelerating voltage.

FT-IR spectroscopy was used to identify the typical bonds in the silica structure with a resolution of 4 cm⁻¹ and range of 280 to 4000 cm⁻¹ (Spectrum 400, Perkin Elmer, United States).

3.5 Manufacturing of the microfluidic device

The microfluidic device was designed using AutoCAD software. The channels had a length of 500 μm and 1000 μm of height. (Figure 9). The microfluidic mold was printed using a 3D printer (Fortus 400mc, Proto3000, Canada) with acrylonitrile butadiene styrene (ABS) polymer. Polydimethylsiloxane (PDMS) was used to manufacture the microfluidic device by using the ESCARGOT (Embedded SCAffold RemovinG Open Technology) technique [27]. SYLGARD silicone elastomer 184 and SYLGARD silicone elastomer 184 curing agent were used to produce the PDMS in a ratio of 10:1 of sylgard 184: curing agent. A 3D printed mold was placed in a glass container avoiding touching the base, then PDMS was poured into the glass container, and placed under vacuum in a desiccator to remove air bubbles for 1 h. The PDMS and the mold were cured for 2 h at 75°C. After that, it was left in acetone for 12 h to dissolve the mold, after which microchannels were cleaned with acetone and dried passing compressed air.



Figure 9. Microfluidic device design.

Under the ESCARGOT methodology device fabrication is easier due to low costs and no need for specialized training in specific equipment. An inconvenient for this methodology is the short range of dimensions that can be used. Depending on the 3D printer, smaller dimensions could not be obtained. For this study, an industrial 3D printer was used to achieve the smallest dimension possible (Figure 10). One of the critical stages in the preparation was the removal of air bubbles. It is important to maintain the solution in vacuum to remove all the bubbles. One of the main drawbacks of ESCARGOT methodology is the irregular printing of the mold. It seems that even when the design must have a smooth shape when the mold is printed it is noticeable the polymer layers that the printer makes. An advantage of this is that the small irregularities in the mold might change the behavior of the fluids in the device by creating small interactive zones. Additionally, these irregularities can help to improve the mixing between the frustules and the

flavonoid. For the experiments, the same device was used to remove a device variation factor for the isorhamnetin encapsulation.

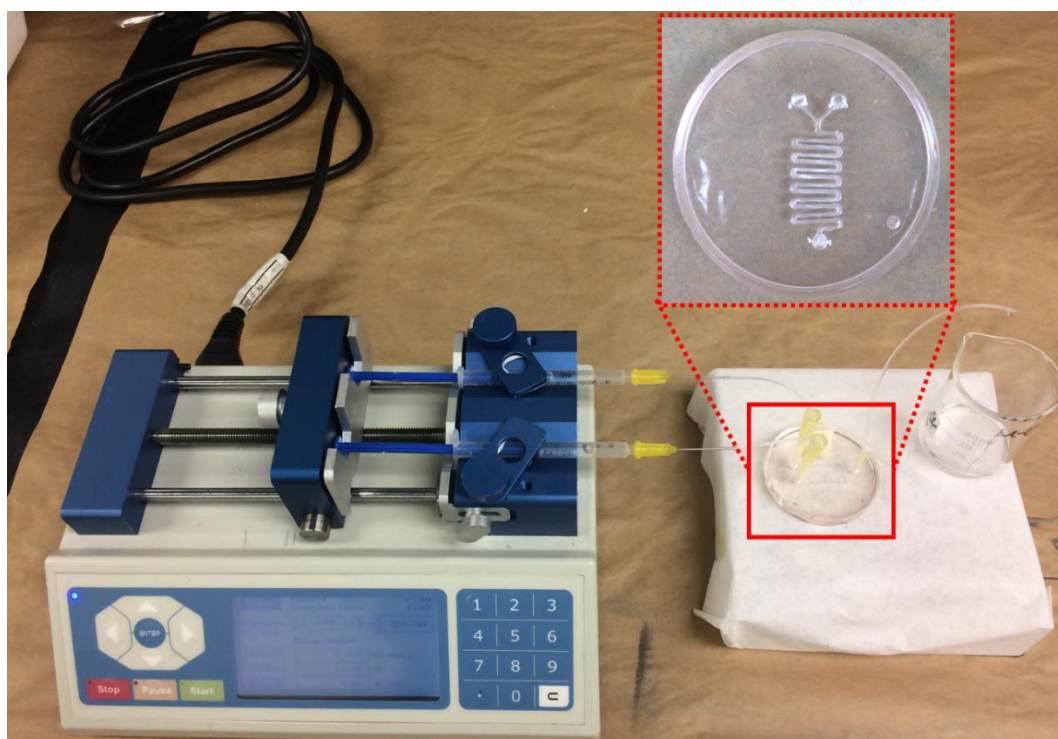


Figure 10. Microfluidic device.

3.6 Isorhamnetin encapsulation

Three different flows were used to modulate the residence time of frustules and drug inside de device, and three different drug concentrations were studied to determine the optimum drug encapsulation conditions (Table 3). A design of experiments was performed to make the statistical analysis of the results (Table A1). A multilevel factorial model (3^k) was used and analyzed with the Desing-Expert software (Version 11, State-Ease, Inc., United States).

Table 3. Factors and levels studied: retention time and drug concentration used.

Residence time (min)	Drug concentration ($\mu\text{g/mL}$)
0.4	20
1	60
2	100

Isorhamnetin concentration that was encapsulated was calculated by absorbance as follow: samples were recollected from the microfluidic device outlet in a 2 mL Eppendorf tube. Samples were centrifuged at 13,000 rpm (Prism R, Labnet International, Inc., United States) for 10 minutes. Supernatant was discarded, and 1.5 mL of distilled water was added to remove non-adsorbed isorhamnetin. Samples were centrifuged and at 13,000 rpm for 15 minutes, and supernatant was removed with a glass Pasteur pipette. 1.5 mL acetone was added to each sample to desorb the isorhamnetin, samples were vortexed for 30 seconds, and tubes were centrifuged at 13,300 for 15 minutes. 700 μ L were placed in a quartz cuvette with a reduced volume. Absorbance was measured from 200-900nm, where the highest peak was detected at 370 nm. Three standard curves of isorhamnetin in acetone were prepared in a range from 0.125 to 16 μ g/mL. Encapsulation efficiency (EE%) and loading capacity were calculated according the following equations:

$$EE\% = \left(\frac{Da-De}{Da} \right) * 100 \quad \text{Eq. 3}$$

$$LC (\%) = \left(\frac{De}{F} \right) * 100 \quad \text{Eq. 4}$$

Where

Da: mass of drug added (μ g)

De: mass of entrapped drug (μ g)

F: frustule weight per sample (μ g)

Samples were analyzed using SEM at 15 V with variable pressure. No gold coating was needed. Samples were placed in a pin with a carbon tape in the surface. Additionally, encapsulation verification was performed by using FT-IR spectrophotometer (Spectrum 400, Perkin Elmer, United States).

3.7 Isorhamnetin release kinetics

Drug release kinetic experiments were performed by using a simulated colonic fluid (SCF). The main components of SCF were 0.2 g/L potassium chloride, 8 g/L sodium chloride, 0.24 g/L potassium phosphate monobasic, 1.44 g/L sodium phosphate dibasic at pH 7 [41]. 30 mL of SCF were placed in a 125 mL Erlenmeyer flask and the samples. Flask was maintained in agitation for 24 h, 37°C, and 50 rpm. Sampling was performed every hour by taking 700 μ L of sample, the

same volume of SCF was added to maintain the same volume during the experiment. Isorhamnetin was measured spectrophotometrically with a range of 200-900 nm, where the highest peak was observed at 240 nm. A standard curve with isorhamnetin was done with 6 points with concentrations ranging from 0.031 to 8 µg/mL using as dissolvent SCF. All experiments were performed in triplicate.

Chapter IV

4. Results and discussion

4.1 Diatom cultivation

As previously mentioned in Chapter II, diatoms use dissolved silicon (in the form of silicic acid) in the medium and transform it into amorphous silicon oxides. Silicon is the only factor that controls the division cell cycle in diatoms. *Cyclotella sp.* was grown in a 5L photobioreactor with a soluble silicon excess in the medium to avoid cell stress. Silicon starvation has shown the production of byproducts such as the accumulation of lipids or production of chitin [58], [60]. In this work, diatom growth exhibited a typical sigmoidal profile and silicon consumption versus cultivation time (Figure 11). A final cell density of 1.16×10^6 cells/mL was achieved after 87 hours of cultivation (Si concentration of 5 mM). The maximum growth rate under the conditions mentioned in the previous chapter was of 0.068 h^{-1} at 40 h. In comparison with other studies, the maximum growth achieved by *Cyclotella sp.* was 0.023 h^{-1} with a perfusion of Si during a semi-continuous cultivation [58], and 1.45 d^{-1} with an initial Si concentration of 6.6 mg/L [61].

In the current study, the intracellular silicon concentration was not measured. In a starvation process, diatoms may not accumulate the intracellular silicon due to the fast intake of soluble silicon from the medium. In an excess silicon medium, the intracellular silicon can be accumulated for a later starvation phase. It was clear that the silicon is needed for cell division, to achieve a higher cell density it a multi-stage silicon addition where diatoms are cultivated in a silicon starvation phase and continue the second stage with a higher concentration of silicon. Additionally, a change in the light intensity and CO_2 to improve the photosynthesis assimilation was used [62].

According to the initial silicon concentration, initial and final cell density, the biomass yield ($Y_{x/s}$) was calculated: 1.59×10^8 cells/mmol Si. As previously mentioned, diatom cell division is dependent on silicon concentration. Depending on the final application, to achieve either a higher or specific biomass yield, the silicon concentration must be simulated and calculated before the experimental work.

A key factor to consider for the final application of frustules is to obtain a homogeneous particle size. One of the main advantages of biosilicification is the production of uniform pores materials in comparison with the critical point in synthetic particle production. It is known that each photoperiod corresponded to one cell division (14 h light and 10 h of darkness). Every cell division,

diatom cells decrease their size due to the separation of the two valves (Figure 4). One of the valves is smaller than the other, hence, during the synthesis of the new valve, the cell decreases its size. When the cell reaches a critical size, the division stops, and the cell starts increasing its original size from the first division. The stationary phase is reached when silicon concentration is depleted. In this period, as cells decrease the division rate, the rest of cells that reached the minimum critical size start to increase the size by using the remnant silicon concentration and/or the internal silicon deposition. Hence, in this study, two photoperiods were required to synchronize cells.

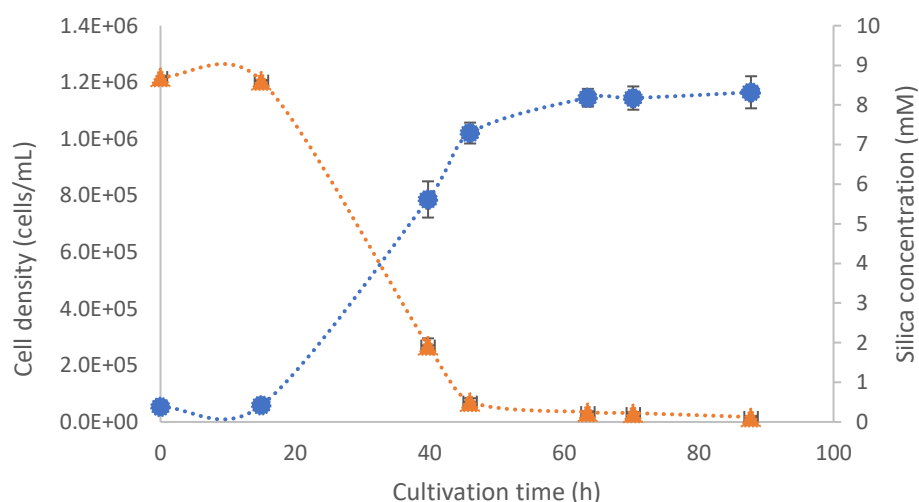


Figure 11. *Cyclotella sp.* growth kinetics.

4.2 Frustule cleaning

The organic material removal from the cell leaves an empty silica shell which is called frustule. Different methodologies remove the organic material that is in the surface and within the cell such as polysaccharides, chitin, amino acid derivatives, and long-chain polyamines [8]. However, the selection of the methodology depends on the final application because some methodologies can cause damage to the frustule. Three methodologies were compared to identify the one which removes more organic material by keeping frustule integrity. In all cases, brown biomass changed color to white. Table 4 shows the results from the methodologies where thermal methodology obtained the highest removal by 100.00%. In this case, all the organic material was carbonized and converted to CO₂, by being a gas, it left the silica without damage. According to the temperature, different molecules are degraded:

around 150°C water evaporation occurred, in a range of 200-600°C a degradation of proteins, oils, polysaccharides and polyamines occurred [63]. This methodology is ineffective to remove metal ions [5]. Thermal degradation at 550°C for 6 h, removes the organic material, however, due to the heating process the negative surface is altered, heat may modify the surface by enlarging the nanopores [64]. For encapsulation and surface functionalization activities, maintaining the negative charge in the surface is vital for the attachment of biomolecules or functional groups. In other studies, similar results were found where the “baking” temperature showed higher organic material removal [5], [65].

The hydrogen peroxide and hydrochloric acid (H₂O₂/HCl) methodology showed a high removal percentage of 45.10%. The acid by an oxidative reaction removed most of the polysaccharides, proteins and some metal ions, hydrogen peroxide helped to dissolve the girdle bands and cause the separation of the two valves. Usually, acid methodologies can change the structure to a stiffer structure while a softer methodology such as SDS/EDTA can provide an elastic material [8].

For the surfactant methodology (SDS/EDTA), the removal obtained was high but not as high as with H₂O₂/HCl. SDS removes the organic material by unfolding proteins and breaking down cell wall proteins and the removal of calcium and other divalent salts with EDTA [66]. As compared with literature, SDS/EDTA resulted in a less efficient methodology to remove organic material [8]. However, the selection of the methodology needs not only has to be chosen according to the application but also depending on the species. For other species, the SDS/EDTA seems to be more suitable than the use of strong oxidative agents as in the case of *Pinnularia sp.* [66], [67].

Centrifugation can provoke the damage of frustules and precipitation of inorganic materials in the sample [68]. In order to obtain intact frustule structures, the removal of the solution should be precipitated and removed by pipetting the sample. Methanol washing helped to remove any pigments remaining in frustules.

SEM images from the three methodologies are shown (Figure 12). It is seen that intact frustules were obtained with all methodologies in comparison with the control (Figure 12A). Control sample consisted of the frustule with no treatment, it had all the organic material. Fractured structures were not observed; the complete valves were detected. Silica shows optical characteristics, specifically in SEM, however, the detection of organic materials using this methodology seems to be less effective than other microscopic techniques. The lack of standardized methodologies for organic material detection is the main drawback to dictate an accurate analysis of this technique. According with these results, the following experiments

were performed with frustules cleaned by the hydrogen peroxide and hydrochloric acid ($\text{H}_2\text{O}_2/\text{HCl}$) methodology. The protocol was performed three times to ensure the total organic removal.

Table 4. Organic material removal.

Methodology	Organic material removal (%)
Thermal	100.00 ± 0.02
$\text{H}_2\text{O}_2/\text{HCl}$	45.10 ± 0.14
SDS/EDTA	40.22 ± 0.19

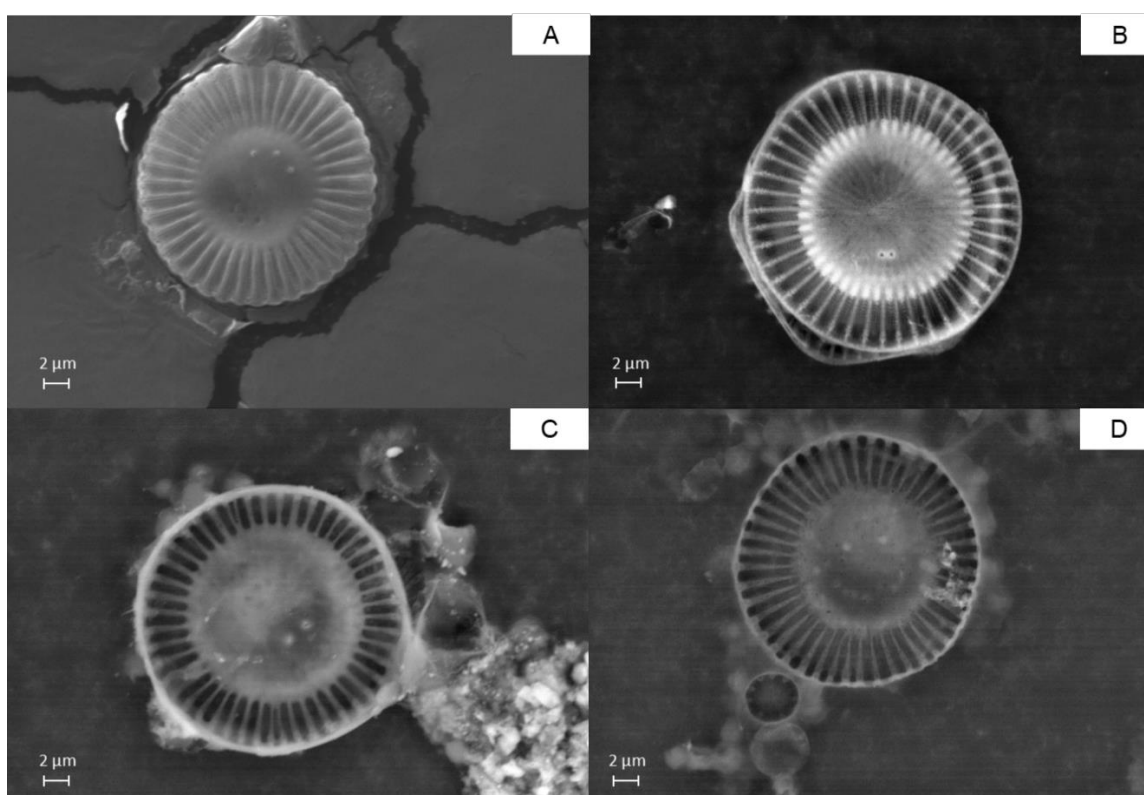


Figure 12. Frustule isolation methodologies. A) Control: original cell with organic material. B) Thermal methodology. C) Acid methodology ($\text{H}_2\text{O}_2/\text{HCl}$). D) Surfactant methodology (SDS/EDTA).

4.3 Frustule characterization

Cyclotella sp. showed a radial and cylindric morphology composed of two valves (Figure 13A). The upper valve had visible pores in the outer rim where chitin is extruded [57]. Larger pores in

the center of the valve where cells attach to each other to form a chain were visible. The centric shape of *Cyclotella* sp. showed rip-shape protuberances in the upper valve. Each rib was composed of several nanopores, and under it, there are layers of them. Diatom cells had an average size of $10.96 \pm 0.02 \mu\text{m}$, the nanopores from the surface were measured at 180 nm on average. Both valves were observed: epitheca (upper valve) and hypotheca (lower valve). Both valves are connected through girdle bands which can be observed as horizontal circumferences (Figure 13B).

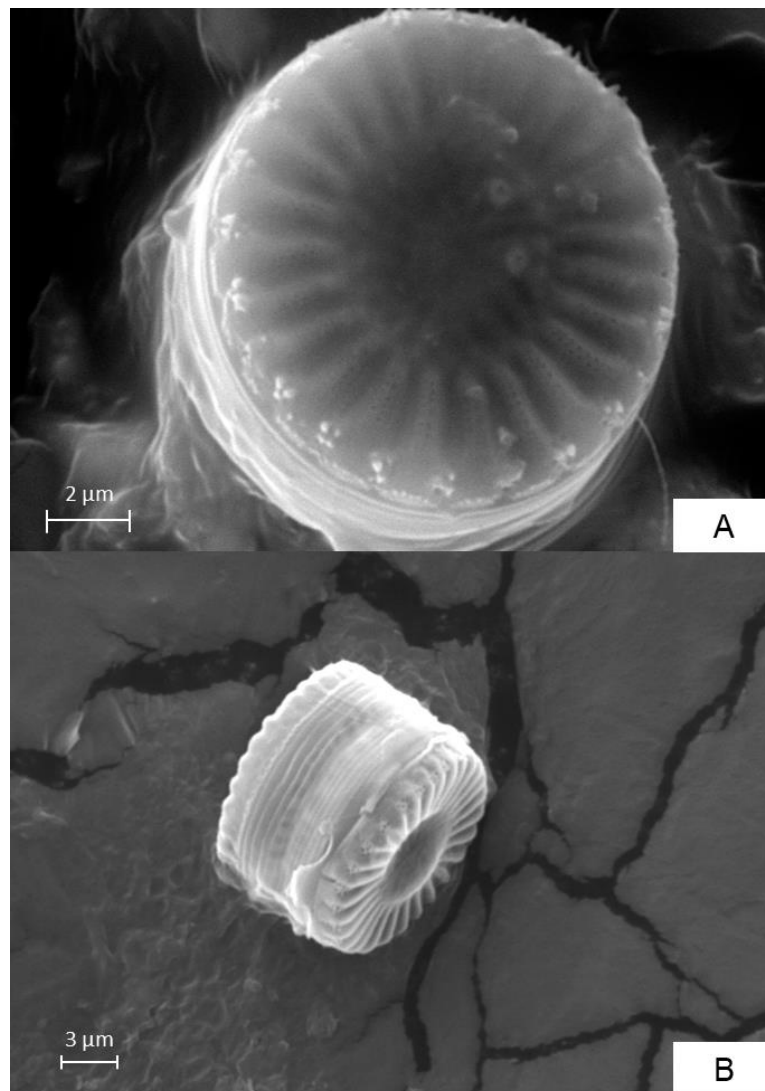


Figure 13. *Cyclotella* sp. SEM images. A) Frontal view of the cell where the nanopores are seen. The bigger pores around the circumference correspond to chitin fiber emerge points. B) Lateral view of the cell where the two valves are observed.

The element analysis displayed 30.53% silicon, 48.84% oxygen, and 20.63% carbon (Figure 14). According to literature, frustules are composed around 90% of silicon and other metals in trace amounts such as aluminum, iron, magnesium, titanium, sodium, phosphorus, manganese, potassium, chromium and calcium [7], [69].

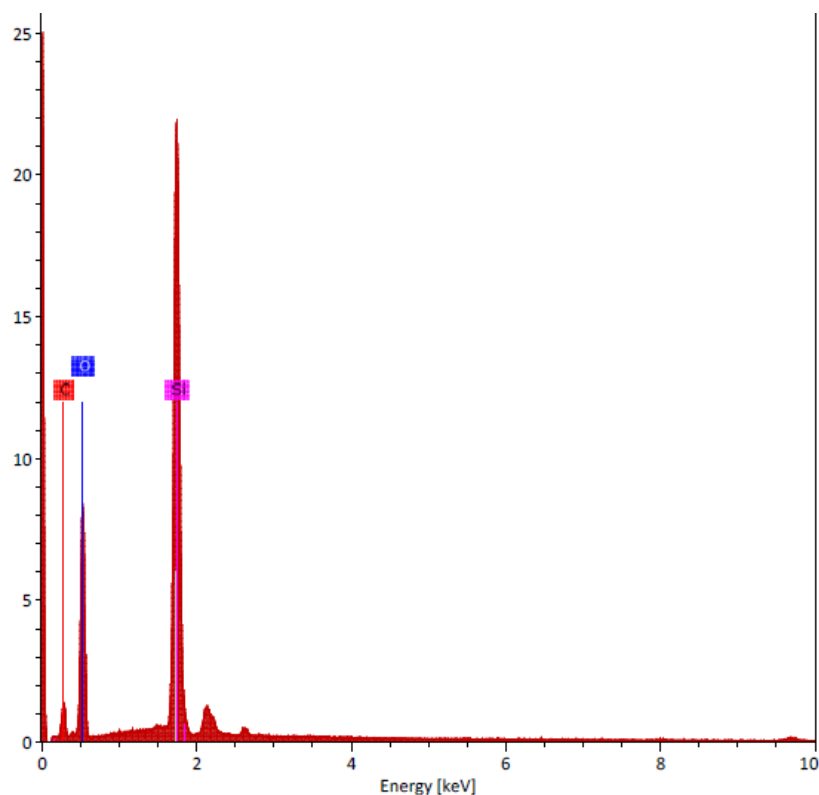


Figure 14. Frustule element analysis.

The FT-IR analysis was performed in a range of 4000-380 cm^{-1} (Figure 15). The typical peaks of Si-O-Si at 461 (bending), 796 (symmetric stretching) and 1100 (antisymmetric stretching) that corresponds to amorphous silica were observed. The crystallization of silica peak appears at 617 cm^{-1} [7], but in the current spectra, the peak is not shown indicating that the amorphous phase was kept during the acid cleaning methodology. The peak at 1632 cm^{-1} corresponded to deformation of an OH bending in water where Si-OH is included as well at the peak 3434 cm^{-1} [5], [65]. The peak at 2919 cm^{-1} corresponded to alkanes [44]. Depending on the resolution of the equipment and the cleaning methodology, usually with a thermal methodology, a peak from 3745 to 3750 cm^{-1} and peak at 3740 cm^{-1} can be observed individually and corresponds to isolated hydroxyl groups (Si-OH) OH vibration of silanol groups [69].

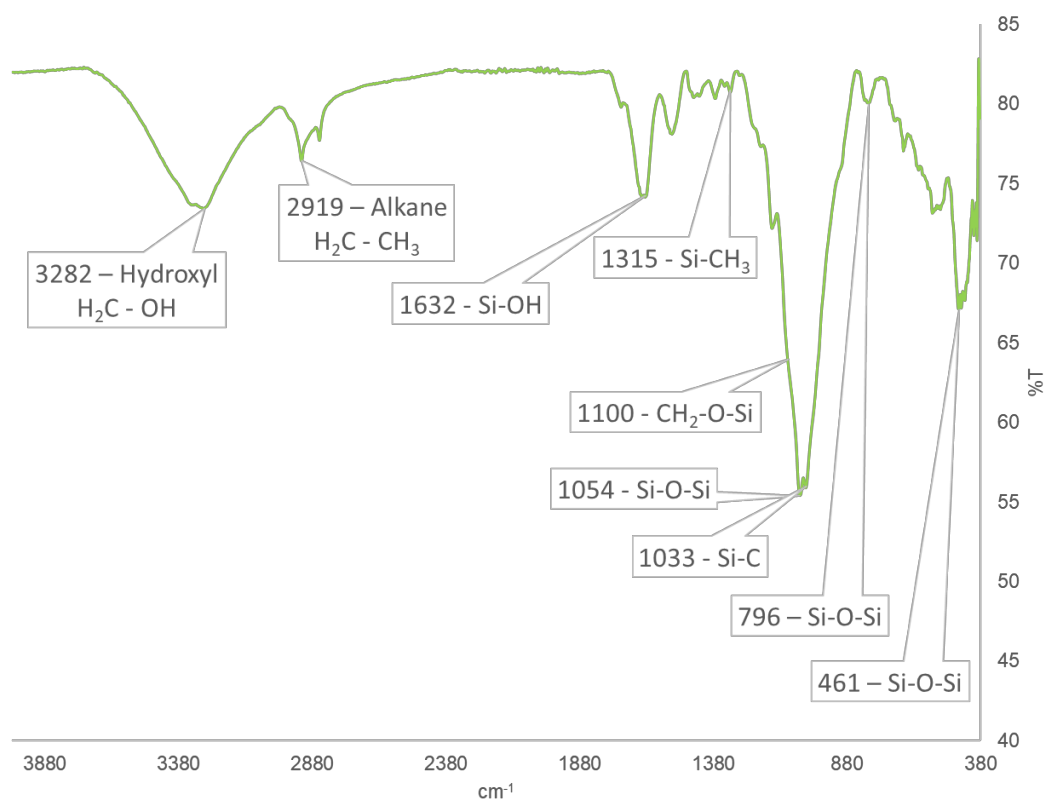


Figure 15. Typical FT-IR spectra of frustules.

4.4 Isorhamnetin encapsulation

Isorhamnetin encapsulation was performed by using a microfluidic device and a syringe pump (Figure 10). Several flows were tested to determine the flow at which frustule particles avoid attachment or agglomeration on the surface of the microchannels (data not shown). A 3^2 design of experiments was used to determine the optimum encapsulation conditions. Two different responses were analyzed: encapsulation efficiency (EE%) and the loading capacity (LC%). The encapsulation efficiency describes the amount of drug that is encapsulated in the carrier over the initial drug concentration; while loading capacity indicates the mass percentage that corresponds to the drug in the total mass. In other words, EE% indicates the ability of the drug to be entrapped, while LC% indicates the ability of the material to entrap a drug.

The residence time inside the device was achieved by modifying the injection flow in the syringe pump. Due to the lack of covalent bonding between the frustule and the isorhamnetin, the encapsulation was performed by adsorption. Therefore, the drug can be easily absorbed or

desorbed from the frustule surface. By increasing the flow, the mixing with the frustule and the drug can have a high diffusion rate. This diffusion rate is dependent on the solubility of the drug with the surface of the carrier.

According to the statistical analysis performed (Table A2), the interaction of the time factor and drug concentration resulted significant ($p < 0.05$) for entrapment efficiency. The mean values of encapsulation efficiency (%) are shown in Figure 16. The highest EE% value obtained was 17.92% (2 minutes, 20 $\mu\text{g/mL}$) followed by 16.40% (0.4 minutes, 20 $\mu\text{g/mL}$). The minimum value obtained was 8.88% (1 minute, 20 $\mu\text{g/mL}$). Regarding the 100 $\mu\text{g/mL}$ concentration, a range of 12-14% was obtained using three different residence times (0.4, 1 and 2 minutes). In comparison, the 60 $\mu\text{g/mL}$ concentration obtained a range of 9-14%. In Figure 16 it is clear that the tendency of a high EE% was when 2 minutes as resident time was used. The optimal conditions to obtain a maximum EE% value were 2 minutes as a resident time in the device and 20 $\mu\text{g/mL}$ of isorhamnetin.

In this case, isorhamnetin is a hydrophobic molecule while the surface of frustules has a hydrophilic, hence the low EE% can be attributed to the physicochemical characteristics of frustules and drug. Additionally, EE% depends on the surface area of the material, the porosity, and available functional groups in the surface (silanol, siloxane groups, or other functional groups added) [70], [71]. However, other studies have reported the EE% in frustules from *Thalassiosira weissflogii* of 0.5% for frustules and 18% functionalized frustule [72]. In comparison with this report, the encapsulation efficiencies were similar but without the functionalization of the surface. Frustules from diatomaceous earth (DE) which are fossilized frustules, were found to reach 94% with no surface modification [45]. As a continuation of the previous report, Aw *et al.*, continued the investigation of 5 different types of surface functionalization methodologies and their effect on EE%; they found a range of 91-97% [73]. Javalkote *et al.* compared the two encapsulation techniques of curcumin (flavonoid) to frustules from *Nitzschia* sp. The results exhibited 73% encapsulation for a non-magnetic frustule versus 41% and 49% for the two methodologies to produce magnetic particles and encapsulate flavonoid at the same time. Here the decrement of the EE% was due to the mass occupied by the magnetic molecule [3].

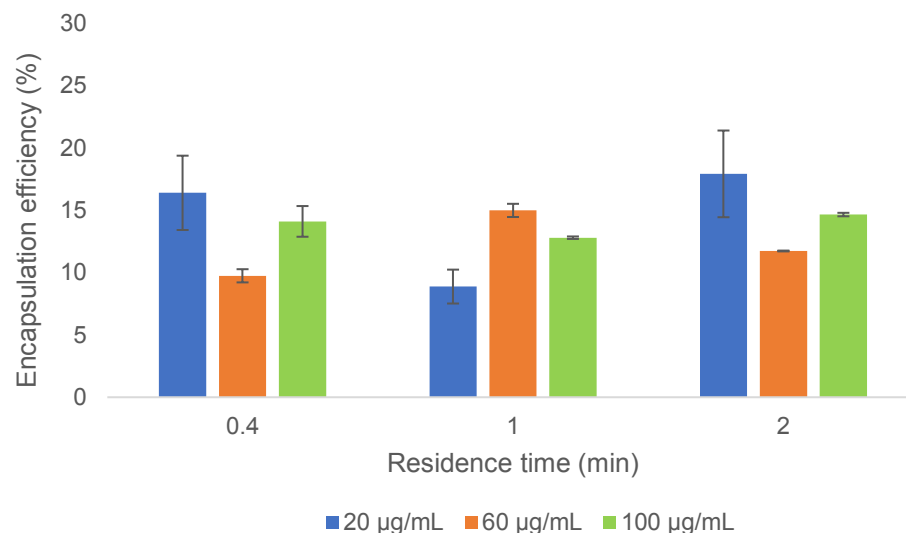


Figure 16. Encapsulation efficiency (%). Error bars represent the standard deviation of triplicates.

For loading capacity (LC%) the results showed an increment when the isorhamnetin concentration increased (Figure 17). The highest value obtained was 1.63% (2 minutes and 100 µg/mL) followed by 1.28 (0.4 minutes and 100 µg/mL). The lowest value was 0.12% (1 minute and 20 µg/mL). For 60 µg/mL, the LC% was in a range of 0.53-0.78%, while for the concentration of 20 µg/mL the values were in a range of 0.12-0.40%. In the statistical analysis, it was exhibited that all the factors and the interaction of them resulted significant ($p < 0.05$). The optimal conditions to maximize the LC% value was the use of 2 minutes and 100 µg/mL isorhamnetin concentration (Table A7). There are similar results obtained with frustules obtained from *Thalassiosira weissflogii* with an LC% of 0.5% and 1.7% for functionalized frustules [72]. In this case, the encapsulation with the microfluidic device avoided the modification of the surface by achieving a similar result as the one reported from Cicco *et al.* However, other studies showed a higher LC% as in the case of the indomethacin drug (hydrophobic) encapsulation in a frustule of diatomaceous earth (DE) were 22% was reported [45]. The same research group, in a further study provided the information of functionalized DE with 5 types of functional groups and obtaining a range of 15-24% [73]. Javalkote *et al.* reported the LC% 14.7% of a flavonoid in frustules, and 8.2 and 9.1% for encapsulation that involved the addition of magnetic material in addition to the flavonoid. Streptomycin was encapsulated in *Coscinodiscus concinnus* frustules by a drop-wise loading methodology achieving a loading capacity of 33.33 % [44]. A comparison between the present study and the literature is presented (Table 5). As previously discussed, the main differences of the LC% are related to the surface and drug characteristics and compatibility among

them. Additionally, in the traditional methodologies, turbulent flows are produced due to the stirring of the drug in solution and frustules. In comparison, in a microfluidic device, the laminar flow in the microchannels may not be enough to create the optimum mixing conditions. The adsorption of biomolecules to frustules relies on the electrostatic interactions, van der Waals forces, and/or hydrophobic interactions [49]. For hydrophobic drugs, it has been reported the addition of functional groups to produce a hydrophobic surface. In this case, the problem of having a hydrophilic surface and hydrophobic drug can be minimized, and the encapsulation efficiency and loading capacity can be maximized.

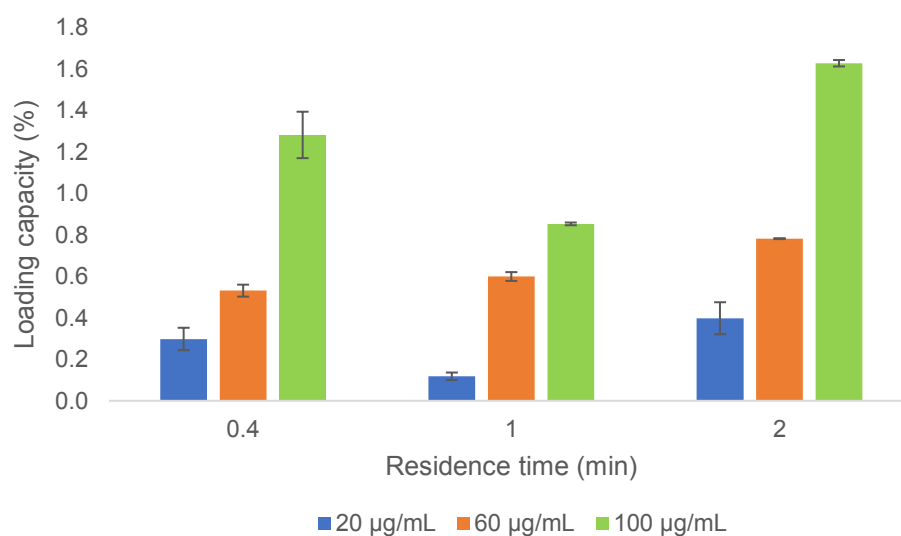


Figure 17. Loading capacity (LC%). Error bars represent the standard deviation of triplicates.

The FT-IR analysis for the frustules, isorhamnetin and encapsulated isorhamnetin is shown in Figure 18. Due to the low amount of isorhamnetin, it was difficult to appreciate the typical peaks of the flavonoid. Aromatic group peaks appeared at 1652 cm^{-1} , while the naphthalene appeared at 1506 cm^{-1} . In the encapsulated isorhamnetin, the naphthalene peak appeared at 795 cm^{-1} . At the peaks of 1629 and 795 cm^{-1} the OH groups of the flavonoid reacted with the groups of the silica.

SEM images of isorhamnetin encapsulation are shown (Figure 19). The brighter points in the surface corresponded to isorhamnetin attached to the surface. A uniform encapsulation was not observed, but rather an heterogeneous dispersion of the flavonoid. This can be attributed to the low intramolecular interactions between the flavonoid and the available functional groups in the silica surface. For the last experiment, optimum conditions for encapsulation were performed.

Table 5. Comparative drug encapsulation.

Marine organism	Frustule size	Frustule shape	Drug	Drug nature	Encapsulation technique	Surface functionalization	%EE	%LC	Ref.
<i>Cyclotella</i> sp.	10.96 ± 0.02 µm	Centric	Isorhamnetin	Hydrophobic	Microfluidic device	No	17.92%	1.63%	Present work
<i>Thalassiosira weissflogii</i>	10-15 µm	Centric	Ciprofloxacin	Hydrophobic	Stirring at 37°C	No	6%	0.5%	[72]
<i>Thalassiosira weissflogii</i>	10-15 µm	Centric	Ciprofloxacin	Hydrophobic	Stirring at 37°C	Yes	18%	1.7%	[72]
<i>Nitzschia</i> sp.	8 µm	Pennate	Curcumin	Hydrophobic	Stirring	No	73%	14.7%	[3]
<i>Nitzschia</i> sp.	8 µm	Pennate	Curcumin	Hydrophobic	Ferrofluid technique	No	41%	8.2%	[3]
<i>Nitzschia</i> sp.	8 µm	Pennate	Curcumin	Hydrophobic	In situ technique	No	49%	9.1%	[3]
Diatomaceous earth (DE)	4-6 µm								
<i>Aulacoseira</i> sp.	diameter, 10-20 µm length	Centric	Indomethacin	Hydrophobic	Drop-wise loading	No	94%	22%	[45]
Diatomaceous earth (DE)	4-6 µm								
<i>Aulacoseira</i> sp.	diameter, 10-20 µm length	Centric	Indomethacin	Hydrophobic	Drop-wise loading	Yes	91-97%	15-24%	[73]
<i>Coscinodiscus concinnus</i>	220 µm	Centric	Streptomycin	Hydrophilic	Drop-wise loading	No	-	33.3%	[44]

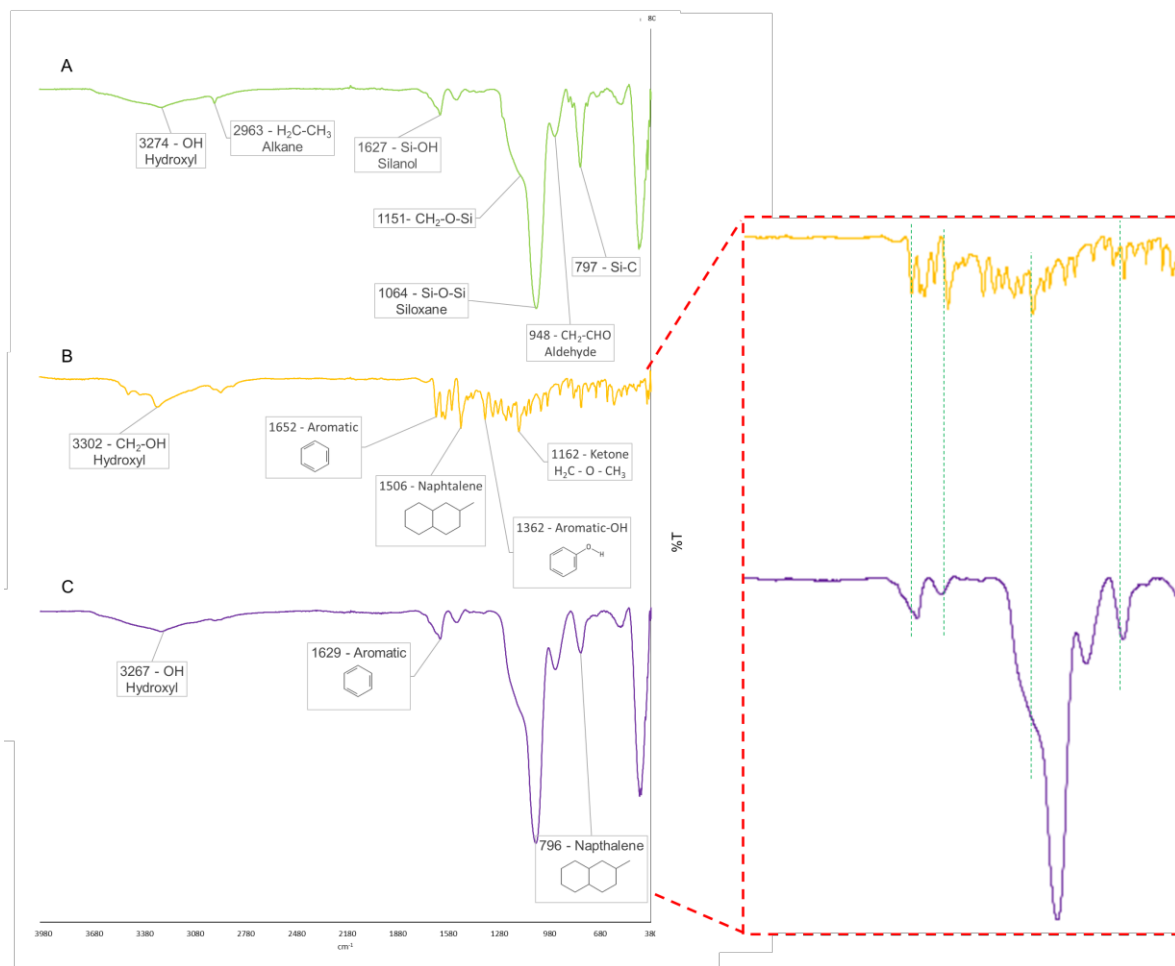


Figure 18. FT-IR spectra of isorhamnetin encapsulated. A) Frustule, B) Isorhamnetin, C) 20 μ g/mL isorhamnetin in frustules.

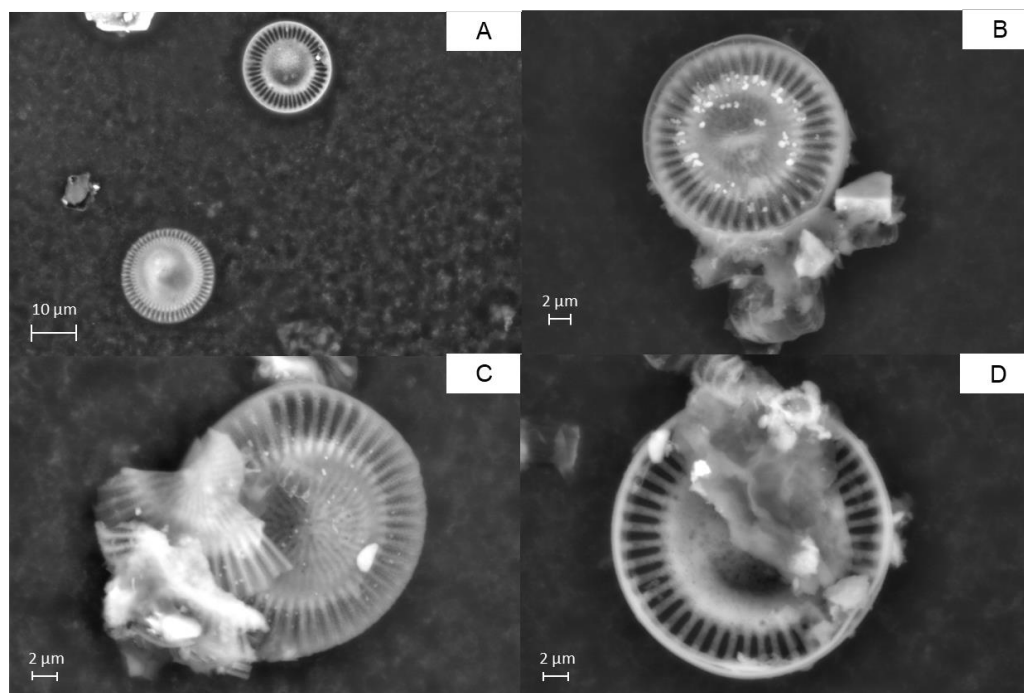


Figure 19. Isorhamnetin encapsulation in different concentrations. A) Control, B) 20 $\mu\text{g/mL}$, C) 60 $\mu\text{g/mL}$ and D) 100 $\mu\text{g/mL}$.

4.5 *In vitro* isorhamnetin release

Drug release studies were performed in a simulated colonic fluid at 37°C. The encapsulation was performed with the optimum conditions according to the statistical analysis from the previous section (2 minutes and 20 $\mu\text{g/mL}$ isorhamnetin concentration). A burst release in the first hour of the study achieving 48.26% was observed (Figure 20). The total release was accomplished after 3 hours of the study. Since the flavonoid was attached to the surface, the release was faster in comparison with the drug that may be attached covalently to a specific functional group. When the drug is placed in the inner pores of the frustule, the release rate from it can be reduced due to the intramolecular interactions between the flavonoid and the silica [74]. It is worth noting that the release rate depends on the nature of the medium, ionic strength of the surface and the drug, and pH. The hydrophobic state of the medium could have retained the release of the flavonoid from the surface; however, due to the low EE% obtained, the drug could have been more prone to be desorbed. Javalkote *et al.*, reported the total release of the curcumin after 12h of the analysis [3]. Several studies reported by using a covalent attachment of the drug to the frustule surface showed a slower and sustained release of the drug of 7 days [72], and 14 days [73]. It has been studied the isorhamnetin pharmacokinetics in beagle dogs and rats.

It was found a half-life ($t_{1/2}$) of 5.4h for beagle dogs and 5.7h for rats, while the time to reach maximum isorhamnetin concentrations in plasma were (T_{max}) 2.6h for beagle dogs, and 6.4-7.21h for rats [75]–[77]. For this study, the drug release in 3h could represent at least 8 hours of therapeutic effect in plasma due the protection effect that the frustule provide to the drug.

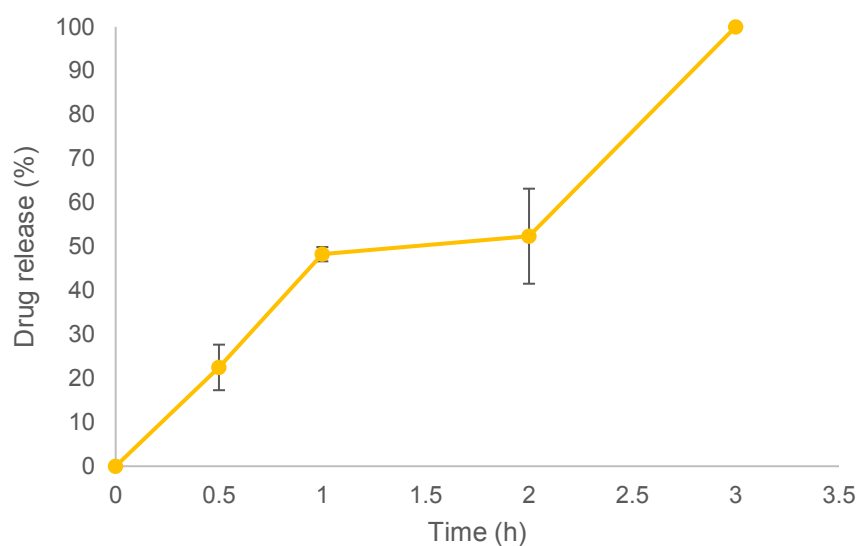


Figure 20. Drug release (%). Bars represent the standard deviation of triplicates.

Chapter V

5. Conclusions

This study reported the use of biogenic silica (frustules) obtained from diatom microalgae to explore their use as carriers for drug delivery. The *Cyclotella* sp. cultivation in photobioreactors allowed to obtain a considerable amount of biomass, and to study cultivation parameters such as growth rate and biomass yield. From the different cleaning methodologies to remove the organic material, the thermal methodology exhibited the best results, though, the main concern was the loss of some OH groups in the surface. SDS/EDTA methodology had the lowest organic material removal. Hence, the best cleaning methodology to maintain OH groups in the surface and the intactness of frustules was with the acid methodology ($\text{H}_2\text{O}_2/\text{HCl}$). Even when several techniques have been described previously, the evaluation of cleaning procedures for a specific specie must be performed to obtain an accurate result. Each diatom specie can react differently to cleaning methodologies, hence the specie, methodology and silica application must be considered. Physicochemical characterization was obtained with high-performance analytical techniques. It was proved that biogenic silica is a good material for drug delivery studies due to its low toxicity, biocompatibility, porosity and rich OH groups.

The ESCARGOT methodology for microdevice fabrication represented a cheap, easy and functional methodology to manufacture microfluidic devices. Drug encapsulation using a microfluidic device allowed to obtain comparable results with traditional methodologies. However, an improvement can be achieved by modifying the geometry of the design to obtain a higher mixing time. The rich OH groups available in frustules were responsible of the encapsulation through intramolecular interactions. Hence, the more time the drug and frustules are in contact, the higher EE%. The mathematical modeling and simulations could be helpful to understand the mixing behavior. The behavior prediction can be used for drugs with different physicochemical characteristics. Interestingly, the encapsulation of two or more drugs can be studied with the aim of a more efficient therapy.

The highest EE% and LC% obtained were 17.92% and 1.63%, respectively. The optimal conditions for encapsulation were 2 minutes as resident time in the microfluidic device and an isorhamnetin concentration of 20 $\mu\text{g}/\text{mL}$. Isorhamnetin release was achieved in 3 hours and according with the isorhamnetin half-life, the therapeutic effect could last up to 5h.

Modifying the surface with functional groups such as amines for the covalent attachment of biomolecules could improve the encapsulation due to a stronger bond and prolong drug release due to slow desorption from frustules. *In vitro* studies in a mammalian cell line for a specific chronic disease should be performed to study the behavior and effects of the isorhamnetin and frustules in a biological assay.

References

- [1] D. Napierska, L. C. J. Thomassen, D. Lison, J. A. Martens, and P. H. Hoet, "The nanosilica hazard: Another variable entity," *Part. Fibre Toxicol.*, vol. 7, no. 39, pp. 1–32, 2010.
- [2] L. Barsanti and P. Gualtieri, "Algal Culturing," in *Algae. Anatomy, Biochemistry and Biotechnology*, Second Edi., Boca Raton: CRC Press, 2014, pp. 221–266.
- [3] V. S. Javalkote, A. P. Pandey, P. R. Puranik, and P. K. Deshmukh, "Magnetically responsive siliceous frustules for efficient chemotherapy," *Mater. Sci. Eng. C*, vol. 50, pp. 107–116, 2015.
- [4] L. Barsanti and P. Gualtieri, "General overview," in *Algae. Anatomy, Biochemistry and Biotechnology*, Second., Boca Raton: CRC Press, 2014.
- [5] W. Jiang *et al.*, "Purification of biosilica from living diatoms by a two-step acid cleaning and baking method," *J. Appl. Phycol.*, vol. 26, no. 3, pp. 1511–1518, 2014.
- [6] C. Jeffryes, T. Gutu, J. Jiao, and G. L. Rorrer, "Two-stage photobioreactor process for the metabolic insertion of nanostructured germanium into the silica microstructure of the diatom *Pinnularia* sp.," *Mater. Sci. Eng. C*, vol. 28, no. 1, pp. 107–118, 2008.
- [7] E. Gulturk and M. Guden, "Thermal and acid treatment of diatom frustules," *J. Achiev. Mater. Manuf. Eng.*, vol. 46, no. 2, pp. 196–203, 2011.
- [8] J. Romann *et al.*, "Diatom frustules as a biomaterial: effects of chemical treatment on organic material removal and mechanical properties in cleaned frustules from two *Coscinodiscus* species," *J. Porous Mater.*, vol. 23, no. 4, pp. 1–6, 2016.
- [9] Y. Xin *et al.*, "Nanoscale drug delivery for targeted chemotherapy," *Cancer Lett.*, vol. 379, pp. 24–31, 2016.
- [10] A. C. Fonseca, A. C. Serra, and J. F. J. Coelho, "Bioabsorbable polymers in cancer therapy: Latest developments," *EPMA J.*, vol. 6, no. 22, pp. 1–18, 2015.
- [11] S. Vishnubhakthula, R. Elupula, and E. F. Durán-Lara, "Recent advances in hydrogel-based drug delivery for melanoma cancer therapy: A mini review," *J. Drug Deliv.*, vol. 2017, pp. 1–9, 2017.
- [12] X. Dong and R. J. Mumper, "Nanomedicinal strategies to treat multidrug-resistant tumors: current progress," *Nanomedicine (Lond)*, vol. 5, no. 4, pp. 597–615, 2010.
- [13] J. Joseph, V. H. B.N., and R. D. D., "Experimental optimization of Lornoxicam liposomes for sustained topical delivery," *Eur. J. Pharm. Sci.*, vol. 112, pp. 38–51, Jan. 2018.

- [14] R. A. Graves, G. A. Ledet, E. Y. Glotser, D. M. Mitchner, L. A. Bostanian, and T. K. Mandal, "Formulation and evaluation of biodegradable nanoparticles for the oral delivery of fenretinide," *Eur. J. Pharm. Sci.*, vol. 76, pp. 1–9, Aug. 2015.
- [15] J. Logie, A. N. Ganesh, A. M. Aman, R. S. Al-awar, and M. S. Shoichet, "Preclinical evaluation of taxane-binding peptide-modified polymeric micelles loaded with docetaxel in an orthotopic breast cancer mouse model," *Biomaterials*, vol. 123, pp. 39–47, Apr. 2017.
- [16] S. Hashemipour and H. Ahmad Panahi, "Fabrication of magnetite nanoparticles modified with copper based metal organic framework for drug delivery system of letrozole," *J. Mol. Liq.*, vol. 243, pp. 102–107, Oct. 2017.
- [17] N. Amreddy *et al.*, "Chemo-biologic combinatorial drug delivery using folate receptor-targeted dendrimer nanoparticles for lung cancer treatment," *Nanomedicine Nanotechnology, Biol. Med.*, vol. 14, no. 2, pp. 373–384, Feb. 2018.
- [18] L. Liang, J.-W. Shen, and Q. Wang, "Molecular dynamics study on DNA nanotubes as drug delivery vehicle for anticancer drugs," *Colloids Surfaces B Biointerfaces*, vol. 153, pp. 168–173, May 2017.
- [19] H. B. Schultz, N. Thomas, S. Rao, and C. A. Prestidge, "Supersaturated silica-lipid hybrids (super-SLH): An improved solid-state lipid-based oral drug delivery system with enhanced drug loading," *Eur. J. Pharm. Biopharm.*, vol. 125, pp. 13–20, Apr. 2018.
- [20] S. Kumar, M. M. Malik, and R. Purohit, "Synthesis Methods of Mesoporous Silica Materials," *Mater. Today Proc.*, vol. 4, no. 2, pp. 350–357, 2017.
- [21] R. Diab, N. Canilho, I. A. Pavel, F. B. Haffner, M. Girardon, and A. Pasc, "Silica-based systems for oral delivery of drugs, macromolecules and cells," *Adv. Colloid Interface Sci.*, vol. 249, no. February, pp. 346–362, 2017.
- [22] P. Tian and Z. Guo, "Bioinspired silica-based superhydrophobic materials," *Appl. Surf. Sci.*, vol. 426, pp. 1–18, 2017.
- [23] D. Y. Zhang, Y. Wang, J. Cai, J. F. Pan, X. G. Jiang, and Y. G. Jiang, "Bio-manufacturing technology based on diatom micro- and nanostructure," *Chinese Sci. Bull.*, vol. 57, no. 30, pp. 3836–3849, 2012.
- [24] M. . Hans and A. . Lowman, "Biodegradable nanoparticles for drug delivery and targeting," *Curr. Opin. Solid State Mater. Sci.*, vol. 6, no. 4, pp. 319–327, 2002.
- [25] E. I. Mancera-Andrade, A. Parsaeimehr, A. Arevalo-Gallegos, G. Ascencio-Favela, and R. Parra-Saldivar, "Microfluidics technology for drug delivery: A review," *Front.*

- Biosci. (Elite Ed)*, vol. 1, no. 10, pp. 74–91, 2018.
- [26] F. Fontana, P. A. M. Ferreira, A. Correia, J. Hirvonen, and H. A. Santos, “Microfluidics as a cutting-edge technique for drug delivery applications,” *J. Drug Deliv. Sci. Technol.*, vol. 34, pp. 76–87, 2016.
- [27] V. Saggiomo and A. H. Velders, “Simple 3D printed scaffold-removal method for the fabrication of intricate microfluidic devices,” *Adv. Sci.*, vol. 2, p. 1500125, 2015.
- [28] F. E. Round and R. M. Crawford, “The Lines of Evolution of the Bacillariophyta. I. Origin,” *Proc. R. Soc. London B Biol. Sci.*, vol. 211, no. 1183, 1981.
- [29] K. W. Jung, D. Jang, and K. H. Ahn, “A novel approach for improvement of purity and porosity in diatomite (diatomaceous earth) by applying an electric field,” *Int. J. Miner. Process.*, vol. 131, pp. 7–11, 2014.
- [30] H. Hajos, M and Stradner, “Late Cretaceous Archaeomonadaceae, Diatomaceae, and Silicoflagellatae from the south pacific ocean, deep sea drilling project, leg 29, site 2751,” *Proc. Ocean Drill. Progr. Sci. Results.*, pp. 913–1009, 1975.
- [31] D. M. Harwood, “Upper Cretaceous and lower Paleocene diatom and silicoflagellate biostratigraphy of Seymour Island, eastern Antarctic Peninsula,” in *Geological Society of America Memoirs*, vol. 169, Geological Society of America, 1988, pp. 55–130.
- [32] D. M. Harwood and R. Gersonde, “Lower Cretaceous Diatoms From Odp Leg 113 Site 693 (Weddell Sea). Part 2: Resting Spores , Chrysophycean Cysts , an Endoskeletal Dinoflagellate , and Notes on the Origin of Diatoms,” *Proc. Ocean Drill. Progr. , Sci. Results*, vol. 113, pp. 403–425, 1990.
- [33] L. K. Medlin, D. M. Williams, and P. A. Sims, “The evolution of the diatoms (Bacillariophyta). I. Origin of the group and assessment of the monophyly of its major divisions,” *Eur. J. Phycol.*, vol. 28, no. 4, pp. 261–275, 2007.
- [34] E. C. Theriot, “A preliminary multigene phylogeny of the diatoms (Bacillariophyta): challenges for future research,” *Plant Ecol. Evol.*, vol. 143, no. 3, pp. 278–296, 2010.
- [35] L. Geitler, “Reproduction and life history in diatoms,” *Bot. Rev.*, vol. I, no. 5, pp. 149–161, 1935.
- [36] J. D. MacDonald, “On the same structure of the diatomaceous frustule and its genetic cycle.,” *Ann. Mag. Nat. Hist.*, vol. 3, no. 13, pp. 1–8, 1869.
- [37] E. Pfitzer, “Untersuchungen über Bau und Entwicklung der Bacillariaceen (Diatomeen),” *Bot Abhandl J Hanstein*, vol. 2, pp. 1–189, 1871.
- [38] G. Drebes, “Sexuality,” in *The biology of the diatoms*, D. Werner, Ed. Oxford: Blackwell Scientific, 1977, pp. 250–283.

- [39] E. Ravera, T. Martelli, Y. Geiger, M. Fragai, G. Goobes, and C. Luchinat, "Biosilica and bioinspired silica studied by solid-state NMR," *Coord. Chem. Rev.*, vol. 327–328, pp. 110–122, 2016.
- [40] M. Sumper and N. Kroger, "Silica formation in diatoms: the function of long-chain polyamines and silaffins," *J. Mater. Chem.*, vol. 14, no. 14, p. 2059, 2004.
- [41] H. Zhang *et al.*, "Diatom silica microparticles for sustained release and permeation enhancement following oral delivery of prednisone and mesalamine," *Biomaterials*, vol. 34, no. 36, pp. 9210–9219, 2013.
- [42] I. Rea *et al.*, "Diatomite biosilica nanocarriers for siRNA transport inside cancer cells," *Biochim. Biophys. Acta - Gen. Subj.*, vol. 1840, no. 12, pp. 3393–3403, 2014.
- [43] J. Janićijević *et al.*, "Inorganically modified diatomite as a potential prolonged-release drug carrier," *Mater. Sci. Eng. C*, vol. 42, pp. 412–420, 2014.
- [44] P. Gnanamoorthy, S. Anandhan, and V. A. Prabu, "Natural nanoporous silica frustules from marine diatom as a biocarrier for drug delivery," *J. Porous Mater.*, pp. 789–796, 2014.
- [45] M. S. Aw, S. Simovic, Y. Yu, J. Addai-Mensah, and D. Losic, "Porous silica microshells from diatoms as biocarrier for drug delivery applications," *Powder Technol.*, vol. 223, pp. 52–58, 2012.
- [46] M. Bariana, M. S. Aw, and D. Losic, "Tailoring morphological and interfacial properties of diatom silica microparticles for drug delivery applications," *Adv. Powder Technol.*, vol. 24, no. 4, pp. 757–763, 2013.
- [47] M. Milović, S. Simović, D. Lošić, A. Dashevskiy, and S. Ibrić, "Solid self-emulsifying phospholipid suspension (SSEPS) with diatom as a drug carrier," *Eur. J. Pharm. Sci.*, vol. 63, pp. 226–232, 2014.
- [48] I. U. Khan, C. A. Serra, N. Anton, and T. Vandamme, "Microfluidics: A focus on improved cancer targeted drug delivery systems," *J. Control. Release*, vol. 172, no. 3, pp. 1065–1074, 2013.
- [49] B. G. Abdallah and A. Ros, "Surface coatings for microfluidic-based biomedical devices," in *Microfluidic devices for biomedical applications*, 1st ed., X. Li and Y. Zhou, Eds. Cambridge: Woodhead Publishing, 2013, pp. 63–99.
- [50] T. yang Wang, Q. Li, and K. shun Bi, "Bioactive flavonoids in medicinal plants: Structure, activity and biological fate," *Asian J. Pharm. Sci.*, vol. 13, no. 1, pp. 12–23, 2018.
- [51] B. song Teng, Y. H. Lu, Z. T. Wang, X. Y. Tao, and D. Z. Wei, "In vitro anti-tumor

- activity of isorhamnetin isolated from *Hippophae rhamnoides* L. against BEL-7402 cells," *Pharmacol. Res.*, vol. 54, no. 3, pp. 186–194, 2006.
- [52] S. K. Ku, T. H. Kim, and J. S. Bae, "Anticoagulant activities of persicarin and isorhamnetin," *Vascul. Pharmacol.*, vol. 58, no. 4, pp. 272–279, 2013.
- [53] M. Antunes-Ricardo, J. A. Gutiérrez-Urbe, F. López-Pacheco, M. M. Alvarez, and S. O. Serna-Saldívar, "In vivo anti-inflammatory effects of isorhamnetin glycosides isolated from *Opuntia ficus-indica* (L.) Mill cladodes," *Ind. Crops Prod.*, vol. 76, pp. 803–808, 2015.
- [54] S. K. Ku, T. H. Kim, S. Lee, S. M. Kim, and J. S. Bae, "Antithrombotic and profibrinolytic activities of isorhamnetin-3-O-galactoside and hyperoside," *Food Chem. Toxicol.*, vol. 53, pp. 197–204, 2013.
- [55] H. J. Lee *et al.*, "Mitochondria-cytochrome C-caspase-9 cascade mediates isorhamnetin-induced apoptosis," *Cancer Lett.*, vol. 270, no. 2, pp. 342–353, 2008.
- [56] P. J. Harrison, R. E. Waters, and F. J. R. Taylor, "A broad spectrum artificial sea water medium for coastal and open ocean phytoplankton," *Journal of Phycology*, vol. 16, no. 1, pp. 28–35, 1980.
- [57] O. G. Chiriboga N. and G. L. Rorrer, "Control of chitin nanofiber production by the lipid-producing diatom *Cyclotella* Sp. through fed-batch addition of dissolved silicon and nitrate in a bubble-column photobioreactor," *Biotechnol. Prog.*, vol. 33, no. 2, pp. 407–415, 2017.
- [58] C. Jeffryes, J. Rosenberger, and G. L. Rorrer, "Fed-batch cultivation and bioprocess modeling of *Cyclotella* sp. for enhanced fatty acid production by controlled silicon limitation," *Algal Res.*, vol. 2, pp. 16–27, 2013.
- [59] K. A. Fanning and M. Pilson, "On the spectrophotometric determination of dissolved silica in natural waters," *Anal. Chem.*, vol. 45, no. 1, pp. 136–140, 1973.
- [60] G. L. Rorrer *et al.*, "The potential of a diatom-based photosynthetic biorefinery for biofuels and valued co-products," *Curr. Biotechnol.*, vol. 5, no. 3, pp. 237–248, Jun. 2016.
- [61] H. M. Shafik, S. Herodek, L. Voros, M. Presing, and K. T. Kiss, "Growth of *Cyclotella meneghiniana* Kütz. I. Effects of temperature, light and low rate of nutrient supply," *Ann. Limnol. - Int. J. Limnol.*, vol. 33, no. 3, pp. 139–147, 1997.
- [62] A. Ozkan and G. L. Rorrer, "Lipid and chitin nanofiber production during cultivation of the marine diatom *Cyclotella* sp. to high cell density with multistage addition of silicon and nitrate," *J. Appl. Phycol.*, vol. 29, no. 4, pp. 1811–1818, 2017.

- [63] D. Lee *et al.*, "Biogenic silica based $Zn_2SiO_4:Mn^{2+}$ and $Y_2SiO_5:Eu^{3+}$ phosphor layers patterned by inkjet printing process," *J. Mater. Chem.*, vol. 18, no. 31, p. 3633, Jul. 2008.
- [64] Y. Wang *et al.*, "Biosilica structures obtained from *Nitzschia*, *Ditylum*, *Skeletonema*, and *Coscinodiscus* diatom by a filtration-aided acid cleaning method," *Appl. Microbiol. Biotechnol.*, vol. 95, no. 5, pp. 1165–1178, 2012.
- [65] Q. I. Yarong, W. Xin, and C. Jay, "Preparation and characteristics of biosilica derived from marine diatom biomass of *Nitzschia closterium* and *Thalassiosira* *," *Chinese J. Oceanol. Limnol.*, vol. 35, no. 3, pp. 668–680, 2017.
- [66] C. Jeffryes, T. Gutu, J. Jiao, and G. L. Rorrer, "Metabolic insertion of nanostructured TiO_2 into the patterned biosilica of the diatom *Pinnularia* sp. by a two-stage bioreactor cultivation process," *ACS Nano*, vol. 2, no. 10, pp. 2103–2112, 2008.
- [67] M. S. Chauton, L. M. B. Skolem, L. M. Olsen, P. E. Vullum, J. Walmsley, and O. Vadstein, "Titanium uptake and incorporation into silica nanostructures by the diatom *Pinnularia* sp. (Bacillariophyceae).," *J. Appl. Phycol.*, vol. 27, no. 2, pp. 777–786, 2015.
- [68] S. Blanco, I. Álvarez, and C. Cejudo, "A test on different aspects of diatom processing techniques," *J. Appl. Phycol.*, vol. 20, no. 4, pp. 445–450, 2008.
- [69] P. Yuan, D. Q. Wu, H. P. He, and Z. Y. Lin, "The hydroxyl species and acid sites on diatomite surface: A combined IR and Raman study," *Appl. Surf. Sci.*, vol. 227, no. 1–4, pp. 30–39, 2004.
- [70] G. W. Lim, J. K. Lim, A. L. Ahmad, and D. J. C. Chan, "Influences of diatom frustule morphologies on protein adsorption behavior," *J. Appl. Phycol.*, vol. 27, no. 2, pp. 763–775, 2015.
- [71] I. Izquierdo-Barba, Á. Martinex, A. L. Doadrio, J. Pérez-Pariente, and M. Vallet-Regí, "Release evaluation of drugs from ordered three-dimensional silica structures," *Eur. J. Pharm. Sci.*, vol. 26, pp. 365–373, 2005.
- [72] S. R. Cicco *et al.*, "Chemically modified diatoms biosilica for bone cell growth with combined drug-delivery and antioxidant properties," *Chempluschem*, vol. 80, no. 7, pp. 1104–1112, 2015.
- [73] M. S. Aw, M. Bariana, Y. Yu, J. Addai-Mensah, and D. Losic, "Surface-functionalized diatom microcapsules for drug delivery of water-insoluble drugs," *J. Biomater. Appl.*, vol. 28, no. 2, pp. 163–174, 2012.
- [74] C. A. Stewart, Y. Finer, and B. D. Hatton, "Drug self-assembly for synthesis of silica

- particles,” *Sci. Rep.*, vol. 8, no. 895, pp. 1–12, 2018.
- [75] J. Duan *et al.*, “A comparison of the pharmacokinetics of three different preparations of total flavones of *Hippophae rhamnoides* in beagle dogs after oral administration,” *Eur. J. Drug Metab. Pharmacokinet.*, vol. 41, pp. 239–249, 2016.
- [76] Z. P. Chen *et al.*, “Comparative pharmacokinetics and bioavailability studies of quercetin, kaempferol and isorhamnetin after oral administration of *Ginkgo biloba* extracts, *Ginkgo biloba* extract phospholipid complexes and *Ginkgo biloba* extract solid dispersions in rats,” *Fitoterapia*, vol. 81, pp. 1045–1052, 2010.
- [77] G. Zhao *et al.*, “Effects of solid dispersion and self-emulsifying formulations on the solubility, dissolution, permeability and pharmacokinetics of isorhamnetin, quercetin and kaempferol in total flavones of *Hippophae rhamnoides* L.,” *Drug Dev. Ind. Pharm.*, vol. 39, no. 7, pp. 1037–1045, 2013.

Annex A

Design of experiments

It is shown the different combination of flow rate and drug concentration for drug encapsulation.

Table A1. Design of experiments.

Exp. #	Time (min)	[Isorhamnetin] (µg/mL)
C1	0.4	0
1	0.4	20
2	0.4	20
3	0.4	20
4	0.4	60
5	0.4	60
6	0.4	60
7	0.4	100
8	0.4	100
9	0.4	100
C2	1	0
10	1	20
11	1	20
12	1	20
13	1	60
14	1	60
15	1	60
16	1	100
17	1	100
18	1	100
C3	2	0
19	2	20
20	2	20
21	2	20
22	2	60
23	2	60
24	2	60
25	2	100
26	2	100
27	2	100

Statistical analysis for encapsulation efficiency

ANOVA for selected factorial model

Table A2. ANOVA for factorial model: encapsulation efficiency.

Source	Sum of Squares	df	Mean Square	F-value	p-value	
Model	141.86	8	17.73	6.40	0.0058	significant
A-Concentration	16.44	2	8.22	2.97	0.1024	
B-Time	19.48	2	9.74	3.52	0.0744	
AB	105.94	4	26.48	9.56	0.0027	
Pure Error	24.94	9	2.77			
Cor Total	166.80	17				

Factor coding is **Coded**.
Sum of squares is **Type II Classical**

The **Model F-value** of 6.40 implies the model is significant. There is only a 0.58% chance that an F-value this large could occur due to noise.

P-values less than 0.0500 indicate model terms are significant. In this case AB is a significant model term. Values greater than 0.1000 indicate the model terms are not significant. If there are many insignificant model terms (not counting those required to support hierarchy), model reduction may improve your model.

Table A3. Fit Statistics.

Std. Dev.	1.66	R ²	0.8505
Mean	13.47	Adjusted R²	0.7176
C.V. %	12.36	Predicted R²	0.4020
		Adeq Precision	7.6811

The **Predicted R²** of 0.4020 is not as close to the **Adjusted R²** of 0.7176 as one might normally expect; i.e. the difference is more than 0.2. This may indicate a large block effect or a possible problem with your model and/or data. Things to consider are model reduction, response transformation, outliers, etc. All empirical models should be tested by doing confirmation runs.

Adeq Precision measures the signal to noise ratio. A ratio greater than 4 is desirable. Your ratio of 7.681 indicates an adequate signal. This model can be used to navigate the design space.

Optimization

9 Solutions found

Solutions for 9 combinations of categorical factor levels

Table A4. Optimization for encapsulation efficiency.

Number	Concentration	Time	Encapsulation efficiency	Desirability	
1	20	2	17.921	0.803	Selected
2	20	0.4	16.400	0.681	
3	60	1	14.990	0.567	
4	100	2	14.657	0.541	
5	100	0.4	14.109	0.497	
6	100	1	12.802	0.392	
7	60	2	11.735	0.306	
8	60	0.4	9.744	0.146	
9	20	1	8.880	0.077	

Statistical analysis for loading capacity

ANOVA for selected factorial model

Table A5. ANOVA for factorial model: Loading capacity.

Source	Sum of Squares	df	Mean Square	F-value	p-value	
Model	3.71	8	0.4643	178.94	< 0.0001	significant
A-Concentration	2.96	2	1.48	571.07	< 0.0001	
B-Time	0.5133	2	0.2566	98.92	< 0.0001	
AB	0.2375	4	0.0594	22.88	< 0.0001	
Pure Error	0.0234	9	0.0026			
Cor Total	3.74	17				

Factor coding is **Coded**.

Sum of squares is **Type II Classical**

The **Model F-value** of 178.94 implies the model is significant. There is only a 0.01% chance that an F-value this large could occur due to noise.

P-values less than 0.0500 indicate model terms are significant. In this case A, B, AB are significant model terms. Values greater than 0.1000 indicate the model terms are not significant. If there are many insignificant model terms (not counting those required to support hierarchy), model reduction may improve your model.

Table A6. Fit Statistics.

Std. Dev.	0.0509	R ²	0.9938
Mean	0.7214	Adjusted R²	0.9882
C.V. %	7.06	Predicted R²	0.9750
		Adeq Precision	41.9279

The **Predicted R²** of 0.9750 is in reasonable agreement with the **Adjusted R²** of 0.9882; i.e. the difference is less than 0.2.

Adeq Precision measures the signal to noise ratio. A ratio greater than 4 is desirable. Your ratio of 41.928 indicates an adequate signal. This model can be used to navigate the design space.

Optimization

9 Solutions found

Solutions for 9 combinations of categoric factor levels.

Table A7. Optimization for loading capacity.

Number	Concentration	Time	Loading capacity	Desirability	
1	100	2	1.629	0.993	Selected
2	100	0.4	1.283	0.767	
3	100	1	0.854	0.488	
4	60	2	0.782	0.441	
5	60	1	0.600	0.322	
6	60	0.4	0.531	0.278	
7	20	2	0.398	0.191	
8	20	0.4	0.298	0.126	
9	20	1	0.118	0.008	

Annex B

Abbreviation list

Table B1. Abbreviation list.

Abbreviation	Description
COC	Cyclic Olefin Copolymer
DDS	Drug Delivery Systems
DE	Diatomaceous Earth
DS	Diclofenac Sodium
EE%	Encapsulation Efficiency
ESCARGOT	Embedded SCAfold RemovinG Open Technology
FTIR	Fourier Transform Infrared Spectroscopy
LC%	Loading Capacity
LCPA	Long-Chain PolyAmines
NPs	Nanoparticles
PC	Poly-Carbonate
PDMS	Poly-DiMethylSiloxane
PEEK	Poly-EtherEtherKetone
PIPR	Polyimide Plastic Resin
PMMA	Poly(Methyl MethAcrylate)
SDV	Silica Deposition Vesicle
SEM	Scanning Electron Microscope
siRNA	Small Interfering RiboNucleic Acid
TOM	Total Organic Material

Published papers

1. **E.I. Mancera-Andrade**, A. Arevalo-Gallegos, A. Parsaeimehr, G. Ascencio-Favela, and R. Parra-Saldívar, “Microfluidics technology for drug delivery: Opportunity and prospects”, *Front. Biosci. Elite*, vol. 10, pp. 74-91, 2018.
2. A. Parsaeimehr, **E.I. Mancera-Andrade**, F. Robledo-Padilla, H.M.N. Iqbal, and R. Parra-Saldívar, “A chemical approach to manipulate the algal growth, lipid content and high value alpha-linoleic acid for biodiesel production”, *Algal Research*, vol. 26, pp. 312-322, 2017.
3. D.A. Esquivel-Hernández, J. Rodríguez-Rodríguez, M. Rostro-Alanis, S.P. Cuéllar-Bermúdez, **E.I. Mancera-Andrade**, J.E. Núñez-Echeverría, J.S. García-Pérez, R. Chandra, and R. Parra-Saldívar, “Advancement of green process through microwave-assisted extraction of bioactive metabolites from *Arthrospira Platensis* and bioactivity evaluation”, *Bioresource Technol.*, vol. 224, pp. 618-624, 2017.
4. D.A. Esquivel-Hernández, J. Rodríguez-Rodríguez, S.P. Cuéllar-Bermúdez, J.S. García-Pérez, **E.I. Mancera-Andrade**, J.E. Núñez-Echeverría, J.E. Ontiveros-Valencia, M. Rostro-Alanis, R.M. García- García, J.A. Torres, W.N. Chen, and R. Parra-Saldívar, “Effect of supercritical carbon dioxide extraction parameters on the biological activities and metabolites present in extracts from *Arthrospira platensis*”, *Mar. Drugs*, vol. 15, no. 6, pp. 174, 2017.
5. L. Sandate-Flores, M.J. Rostro-Alanis, **E.I. Mancera-Andrade**, D.A. Esquivel-Hernández, C. Brambila-Paz, R. Parra-Saldívar, J. Welte-Chanes, and Z. Escobedo-Avellaneda, “Using high hydrostatic pressures to retain the antioxidant compounds and to reduce the enzymatic activity of pitaya-pineapple (*Stenocereus sp. – Fragaria ananassa*) beverage”, *J. Food Sci. Tech.*, vol. 54, no. 3, pp. 611-619, 2017.
6. F. Ruiz-Ruiz, **E.I. Mancera-Andrade**, R. Parra-Saldívar, T. Keshavarz, and H.M.N. Iqbal, “Drug delivery and cosmeceutical applications of poly lactic acid based novel constructs – A review”, *Curr. Drug Metab.*, vol. 18, no. 10, pp. 914-925, 2017.

7. F. Ruiz-Ruiz, **E.I. Mancera-Andrade**, and H.M.N. Iqbal, "Marine-derived bioactive peptides for biomedical/pharmaceutical sectors – A mini review", vol. 24, no. 2, pp.9, 2016.
8. M.J. Rostro-Alanis, **E.I. Mancera-Andrade**, M.B. Gómez-Patiño, D. Arrieta-Baez, S.O. Martínez-Chapa, B. Cardenas, and R. Parra-Saldívar, "Nanobiocatalysis: Nanostructured materials" *Biocatalysis*, vol. 2, pp. 1-24, 2016.

Book Chapter

1. R. Chandra, C. Castillo-Zacarias, **E.I. Mancera-Andrade**, S.V. Mohan, and R. Parra-Saldívar, "Fundamentals of biophotovoltaics for conversion of solar energy to bioelectricity" in *Microbial electrochemical technology: Platform for fuels, chemicals and remediation*, first edi., Elsevier, 2018.

VITA

Elena Ivonne Mancera Andrade was born in Xalapa, Veracruz, Mexico on 2nd March 1990. She earned a Biotechnology Engineering degree from Tecnológico de Monterrey, campus Monterrey (ITESM) in 2014. During her Bachelor studies, she was part of several activities such as vice president of Kairos student group, participation as staff in NUCLEUM conferences, social service activities, and sport activities. In 2014, she worked as a research assistant in the NutriOmics group and Water Center for Latin America both at Tecnológico de Monterrey, campus Monterrey.

From January 2015 to July 2016 she worked as a research assistant at Emerging Technologies and Molecular Nutrition group at Tecnológico de Monterrey in the development of funded projects. During this stage, she published 3 research articles and 3 review articles, and she participated in 3 international conferences, and 2 courses of biocatalysis.

In August 2016, she was accepted in the Master of Science in Biotechnology program at Tecnológico de Monterrey, campus Monterrey. During her Master studies, she did an internship at Oregon State University at Dr. Gregory Rorrer's Lab in Corvallis, Oregon, United States from August 2017 to December 2017. She published 1 research article, 1 review article and 1 book chapter, and she participated in two international conferences where a poster and oral presentations were achieved.

This document was typed in using Microsoft Word by Elena Ivonne Mancera Andrade.